Assimilation of T-TREC-Retrieved Wind Data with WRF 3DVAR for the Short-term Forecasting of Typhoon Meranti (2010) near Landfall

Xin Li, Jie Ming, Yuan Wang, Kun Zhao
[1]Key Laboratory for Mesoscale Severe Weather/MOE and School of Atmospheric Science, Nanjing University, Nanjing 210093, China

Ming Xue
[2]Center for Analysis and Prediction of Storms, and School of Meteorology, University of Oklahoma, Norman, Oklahoma, USA, 73072

April, 2013

Submitted to Journal of Geophysical Research

Revised July, 2013

Corresponding author address:

Dr. Jie Ming
Key Laboratory for Mesoscale Severe Weather/MOE and School of Atmospheric Science, Nanjing University, Nanjing 210093, China
jming@nju.edu.cn

Abstract

An extended Tracking Radar Echo by Correlation (TREC) technique, called T-TREC technique, has been developed recently to retrieve horizontal circulations within tropical cyclones (TCs) from single Doppler radar reflectivity (Z) and radial velocity (V_r, when available) data. This study explores, for the first time, the assimilation of T-TREC-retrieved winds for a landfalling typhoon, Meranti (2010), into a convection-resolving model, the WRF (Weather Research and Forecasting). The T-TREC winds or the original V_r data from a single coastal Doppler radar are assimilated at the single time using the WRF 3DVAR, at 8, 6, 4 and 2 hours before the landfall of typhoon Meranti. In general, assimilating T-TREC winds results in better structure and intensity analysis of Meranti than directly assimilating V_r data. The subsequent forecasts for the track, intensity, structure and precipitation are also better, although the differences becomes smaller as the V_r data coverage improves when the typhoon gets closer to the radar. The ability of the T-TREC retrieval in capturing more accurate and complete vortex circulations in the inner-core region of TC is believed to be the primary reason for its superior performance over direct assimilation of V_r data; for the latter, the data coverage is much smaller when the TC is far away and the cross-beam wind component is difficult to analyze accurately with 3DVAR method.

1. Introduction

Accurate prediction of the track, intensity, structure and precipitation of landfalling tropical cyclones (TCs) is crucial for the protection of life and property. In the past years, TC track forecasting has improved steadily [Rappaport et al. 2009] with significant contributions from satellite or other non-traditional observations and improved numerical models, but the intensity and structure forecasting has improved much more slowly [Houze et al. 2007]. One of the primary reasons is that the inner-core structures of TC are often inadequately initialized in operational models, while such structures are believed to be important for intensity forecasting.

Many efforts have been made to improve the initial conditions focusing on the data assimilation (DA) by using different types of observations from various platforms. Assimilating typhoon bogus data (BDA) has been shown to result in much better intensity forecast [e.g., Zou and Xiao 2000; Xiao et al. 2009a]. Such a method relies significantly on the empirical profiles of sea level pressure (SLP) and/or wind assumed in the bogus vortex and therefore cannot represent the true TC structure. Studies have shown that the assimilation of satellite wind and aircraft dropsonde data helps to improve the environmental conditions and track forecast of TCs [Pu et al. 2008; Chou et al. 2011]. Among the various observational platforms, Doppler radar is the only platform that can observe the three-dimensional structure of TCs with high temporal and spatial resolutions. The airborne Doppler radar data have been shown to allow for the analyses of the inner core structure of TCs, especially during their lifetime over the ocean, which lead to improve track as well as intensity forecasting [Pu et al. 2009; Xiao et al. 2009b; Du et al 2012; Weng and Zhang 2012]. For landfalling TCs, coastal ground-based Doppler radars are commonly used for TC monitoring and forecasting. Several recent studies have shown that the direct assimilation of radar Radial Velocity (V_r) data into cloud-resolving numerical models can improve TC analysis and forecasting [e.g., Xiao et al. 2005; Zhao and Xue 2009; Zhang et al. 2009; Dong and Xue 2012]. All the studies cited above use either three-dimensional variational (3DVAR) or ensemble Kalman filter (EnKF) method for data assimilation. Compared with EnKF, 3DVAR is more computationally efficient and suitable for operational use. However, 3DVAR typically does not analyze the cross-beam components of wind well from single-Doppler radar radial velocity data especially when it is not used in a cycled mode.

Instead of assimilating the original V_r data, assimilating retrieved winds can be more effective. Zhao et al. [2011] explored the assimilation of winds retrieved using the GBVTD [Ground-based velocity track display, Lee et al. 1999] method for super typhoon Saomai (2006) near its landfall. The 3DVAR assimilation of GBVTD-retrieved winds data resulted in better structure, intensity and precipitation analysis and forecasts of Saomai than direct assimilation of V_r data, partly because the GBVTD method can provide the full circle of vortex circulation in the inner-core region while V_r data coverage is often incomplete. However, due to the geometric limitation imposed in GBVTD, the analysis domain is limited to the region satisfying $R/R_T<0.7$, where R is the radius of the analysis ring and R_T is the distance of the TC center from the radar. In addition, for most operational radar, such as the WSR-88D of the U.S., and WSR-98D of China, the maximum Doppler velocity range is about 230 km, far less than the maximum range of reflectivity, Z data, which is typically 460 km. It would thus be advantageous if the reflectivity data could be used to estimate the wind field to provide data coverage when the TC is further away from the coast.

Tuttle and Gall [1999] successfully retrieved TC circulations using reflectivity data from two consecutive PPI (Plan Position Indicator) scans with the tracking radar echoes by correlation (TREC) method. Wang et al. [2011] developed the so-called TC circulation TREC (T-TREC) technique by extending TREC to a polar coordinate centered at the TC center with the vortex rotating rate estimated from V_r data as an extra retrieval condition. This condition provides a constraint on the searching range for spatial correlation in T-TREC algorithm, and helps reduce the wind underestimation problem often encountered in the eyewall region where the reflectivity is often relatively uniform along the eyewall rainband [Tuttle and Gall 1999]. This study explores for the first time the assimilation of T-TREC-retrieved wind data from a single radar located at Xiamen (XMRD) of Fujian Province, China, for typhoon Meranti (2010) that experienced a sudden intensification near the coast of China and brought heavy rainfall to coastal Fujian and Zhejiang Provinces. The used data assimilation system is the WRF (Weather Research and Forecasting) 3DVAR [Baker et al. 2003].

Four pairs of data assimilation experiments are performed, with each pair containing one experiment assimilating V_r data and one assimilating T-TREC data. These pairs analyze for the single-time of radar data at 1200, 1400, 1600 and 1800 UTC, 9 September 2010, respectively. The 1200 UTC is the time when the inner core region of typhoon Meranti first moved into the full coverage of XMRD reflectivity data but was only partially covered by the radial velocity data. This is also about the earliest time when T-TREC-retrieved wind retrieval can be successfully performed. The other experiments starting at the later times examine the relative impacts of T-TREC-retrieved winds versus V_r data when the typhoon was closer to the radar to have better V_r coverage. To focus on the impact of the original V_r and the retrieved T-TREC wind data, all experiments excluded the assimilation of Z data.

The rest of this paper is organized as follows. Section 2 describes the radar data, forecasting model, assimilation system and experimental configurations. Sections 3 and 4 examines the impacts of assimilating V_r data versus T-TREC-retrieved winds on the track, intensity and structure forecasting of Meranti during and after landfall; the results are compared to a forecast starting from the National Centers for Environmental Predication (NCEP) operational Global Forecast System (GFS) analyses at 1200 UTC without any radar data assimilation. Section 3 discusses in detail the results from the 1200 UTC experiments while section 4 presents results from the experiments with later analysis times. Summary and conclusions are presented in Section 5.

2. Method and experimental design

2.1 Radar V_r and T-TREC-retrieved wind data

In this paper, Level II data from XMRD radar are used, and the radar is located at the southeastern coast of China (Fig. 1). V_r and Z data are edited manually using NCAR Solo software [Oye et al., 1995] to remove/correct erroneous radar observations, including velocity dealiasing and ground clutters. The radial resolutions of the original XMRD radar data are 0.25 km for V_r and 1 km for Z, respectively. The V_r data are thinned to a 4 km grid before assimilation. For T-TREC retrieval [Wang et al. 2011], quality controlled Z and V_r data are first interpolated to a grid with 1 km horizontal and vertical grid spacings, then the retrieval is performed within a 300 km radius from the TC center, in cylindrical-polar coordinates. The T-TREC retrieval procedure [Wang et al. 2011] as used in this study is briefly described in the following.

As in the traditional TREC method, T-TREC uses Z data from two consecutive scan times T_1 and T_2 (6 minutes apart in this study). The analysis divides each scan into the same number of arc-shaped cells. Each cell from the first scan is cross-correlated with all possible cells in the second scan. The coefficient ρ_z is calculated by using the formula of Tuttle and Gall (1999),

$$\rho_z = \frac{\sum_{k=1}^{N} Z_1(k) Z_2(k) - \frac{1}{N}\sum_{k=1}^{N} Z_1(k) \sum_{k=1}^{N} Z_2(k)}{[(\sum_{k=1}^{N} Z_1^2(k) - N\overline{Z_1}^2)(\sum_{k=1}^{N} Z_2^2(k) - N\overline{Z_2}^2)]^{\frac{1}{2}}}, \qquad (1)$$

where Z_1 and Z_2 are Z arrays at T_1 and T_2, respectively, and N is the number of data points within a cell.

To reduce the uncertainty produced by subjective selection of searching area, the V_r is used to improve the estimation of the searching range and to create a velocity correlation coefficient. As the TC circulation exhibits a distinct dipole pattern on Doppler radial velocity images and with the TC circulation being modeled by a Rankine vortex [Brown and Wood, 1983], the mean tangential wind component $V_T(R)$ at each radius from TC center can be estimated by

$$V_T(R) = \frac{|V_{r\max}(R)| + |V_{r\min}(R)|}{2}, \qquad (2)$$

where R is the distance from the TC center, and $V_{rmax}(R)$ ($V_{rmin}(R)$) is the maximum (minimum) outbound (inbound) radial velocity. Therefore, a reference searching distance in the azimuth direction D_{Aref} (OR as shown in Fig. 2a) and that in the radial direction D_{Rref} (half of $\overline{AB}$ as shown in Fig. 2a) can be defined as

$$D_{Aref} = V_T(R) \cdot \Delta t \,, \qquad (3)$$

$$D_{Rref} = \alpha \cdot V_T(R) \cdot \Delta t \,, \qquad (4)$$

Since the magnitude of radial flow is typically an order of magnitude smaller than the tangential flow within a TC [Roux and Marks 1996], parameter α is set to 0.3, as in Wang et al. [2011]. Based on the reference searching distance in the azimuth direction, an additional wind weight coefficient ρ_v is defined as

$$\rho_v = \begin{cases} 1, & D_{Aref}(1-\beta) \le D_A \le D_{Aref}(1+\beta) \\ 0, & others \end{cases} , \qquad (5)$$

Considering that the real tangential velocity may fluctuate around $V_T(R)$ and the axisymmetric component of tangential velocity is typically an order of magnitude larger than the asymmetric component [Roux and Marks 1996], β is used as an adjustable parameter and set to 0.3, as in Wang et al. [2011].

By combining the reflectivity correlation coefficient ρ_z with the wind weight coefficient ρ_v, a new, final, correlation coefficient is given by

$$\rho = \rho_z \rho_v \,, \qquad (6)$$

The final correlation coefficient ρ confines the actual search area to a limited area with non-zero coefficient (hatching area in Fig. 2a). When V_r is unavailable, $\rho = \rho_z$, the T-TREC method reduces to the traditional TREC method [Tuttle and Gall 1999; Harasti et al. 2004]. The location of target cell (Fig. 2b) that has the highest correlation coefficient represents the end point of the retrieval vector. The wind vector is estimated by the arc length between the initial and target cells and their time interval. The estimated velocities are interpolated to a Cartesian grid with 10 km horizontal and 1 km vertical grid spacings in the end.

2.2 WRF model and WRF 3DVAR

The Advanced Research WRF (ARW) [Skamarock et al. 2008] with full physics is used during the DA and for the forecast. Three two-way nested domains are employed. The domains have horizontal dimensions of 258×238, 463×463 and 616×616, and grid spacings of 12, 4 and 1.33 km, respectively. All model domains have 35 vertical levels from the surface to 50 hPa. The physics options include the Purdue Lin microphysics [Lin et al. 1983; Chen and Sun 2002], RRTM longwave radiation [Mlawer et al. 1997], Dudhia shortwave radiation [Dudhia 1989], Monin-Obukhov surface-layer [Monin and Obukhov 1954], Noah land-surface [Chen and Dudhia 2001], and YSU planetary boundary layer [Nohet et al. 2003] schemes. The Kain-Fritsch cumulus scheme [Kain and Fritsch 1990; Kain 2004] is only used on the 12-km domain. GFS analyses with a 0.5° spacing are used to provide the boundary conditions, and as the analysis background for the DA experiments or as the initial condition for the non-DA experiment.

In the WRF-3DVAR system, the ‘CV5’ background error option is used with the control variables of stream function, unbalanced velocity potential, unbalanced surface pressure, unbalanced temperature and relative humidity. The background error covariances matrix (BE matrix) is generated via the National Meteorological Center (NMC) method [Parrish and Derber 1992] for our own forecasting domain sampling from one month forecasts. It allows for separate definition of both horizontal and vertical correlation functions, and the multivariate covariance between different variables is represented via statistical regression.

2.3 Experimental design

For comparison purpose, a baseline control forecast (CTL), using the GFS analysis at 1200 UTC, 9 September as the initial condition (IC) is first performed. The GFS analyses include surface observations, radiosondes, cloud-track winds, aircraft observations, satellite-based Global Positioning System (GPS) radio occultation and satellite radiances [Hamill et al. 2011] but not ground-based radar data. As briefly descried earlier, the first pair of experiments, ExpVr and ExpTrec (Table 1), assimilates V_r and T-TREC data using WRF 3DVAR at 1200 UTC, 9 September 2010, when the inner core region of typhoon Meranti first moved into the full coverage of XMRD reflectivity data (Fig. 1b) but was still beyond the full coverage of radial velocity data (Fig. 1a). The impacts of assimilating T-TREC wind versus V_r data on the analysis and forecasting of the structure, intensity and track of Meranti during 18 hour period are discussed in detail in section 3.

To examine the relative impacts of T-TREC and V_r data at later times when the TC was closer to the radar, three additional pairs of experiments starting at 1400, 1600 and 1800 UTC (see Table 1) are performed and discussed in section 4. For these experiments, the analyses use the forecasts of CTL valid at the corresponding times as the analysis background.

Within the 3DVAR analysis, the standard deviations of the observational errors for V_r and T-TREC-retrieved wind data are prescribed to be 1.5 m s^{-1} and 4 m s^{-1}, respectively. Similar to those used in earlier studies [e.g., Zhao and Xue 2009; Zhao et al. 2012; Dong et al. 2012], the V_r error includes instrumental error which is mainly due to spatial inhomogeneities in velocity and reflectivity within a radar sampling volume. It also includes representativeness error and errors due to data quality issues. For estimating the T-TREC wind retrieval error, the root mean square difference (RMSD) between the retrieved V_r (obtained by projecting T-TREC winds onto the radar radial directions) and the observed V_r is calculated. The error of the T-TREC retrieved winds is roughly estimated as the sum of the RMSD and the V_r error. Figure 3 shows the percentage histogram of the absolute difference between the retrieved and observed V_r, and a scattered diagram of the two during the entire retrieval period for Meranti. The percentage of wind differences of less than 4 m s^{-1} is about 75% while the overall RMSD is 2.6 m s^{-1}. We therefore specify the T-TREC retrieval error to be 4 m s^{-1}, which is in agreement with the statistics of data samples in Wang et al. [2011]. Overall, we see that correlation between the retrieved and observed V_r is as high as 0.96, suggesting the quality of the retrieval is rather good (Fig. 3).

The procedure for assimilating V_r data in this study is similar with that described in Xiao et al. [2005] and Xiao and Sun [2007]. The retrieved T-TREC winds are horizontal wind components and are treated as sounding winds as was done with airborne Doppler radar wind retrieval in Xiao et al. [2009b]. For realistic analysis of TC circulations, the default horizontal background covariance correlation scale derived from the NMC method in WRF-3DVAR is scaled by a factor of 0.15, following Li et al. [2012], resulting a de-correlation scale of about 20 km, similar to that used in Zhao et al. [2012] with the ARPS 3DVAR [Xue et al. 2003]. Without the correlation scale adjustment, the 3DVAR produces unrealistic wind increments, as shown in Li et al. [2012], because the NMC-method derived correlation scales reflect mainly synoptic-scale error structures. The data assimilation is performed on the 4-km domain and the analyses are transferred to the other two grids in the two-way interactive configuration. Only results on the 1.33-km domain will be presented because they contain most details.

3. Results of experiments with 1200 UTC analysis time

In this section, we present and discuss the analysis and forecast results from experiments ExpVr and ExpTrec that analyze V_r and T-TREC data, respectively, at 1200 UTC, and the results are also compared to those of experiment CTL that does not assimilate any radar data.

3.1. Impact on the analyzed TC structures

At the assimilation time of 1200 UTC, 9 September, Meranti is in category 1 and the maximum surface wind speed from Chinese Meteorological Administration (CMA) best track data is 33 m s^{-1}. Figures 4a-c show the horizontal winds at 3-km height from CTL, ExpVr and ExpTrec at 1200 UTC. Apparently, the typhoon circulation directly from GFS analysis in CTL (Fig. 4a) is very weak with a broad eye. The main difference of the vortex circulation between ExpVr (Fig. 4b) and CTL takes place in the northern part of typhoon, indicating that the direct assimilation of V_r data for a single time has only local adjustments on the vortex structure. This can be largely attributed to the limited coverage of V_r data at this time (see Fig. 1a). The maximum wind in the inner core region in ExpVr is enhanced to 27 m s^{-1} in the northeastern quadrant, versus less than 10 m s^{-1} in CTL. Compared with ExpVr, ExpTrec (Fig. 4c) produces a much tighter and stronger circulation in the inner core region. The highest wind speed is also located in the northeastern quadrant of the vortex, with a maximum wind speed of 30 m s^{-1} at this level. To confirm the better quality of the analyzed circulation in ExpTrec, we projected the analyzed winds onto the radial directions of Taiwan Chi-Gu (RCCG) radar (the location of RCCG is shown in Figs. 4a, b, c) to obtain analyzed V_r data and compared the data against RCCG V_r observations. The calculated RMSDs for CTL, ExpVr and ExpTrec are 13.9, 6.1 and 3.8 m s^{-1}, respectively, with that of ExpTrec being clearly the smallest. It is worth pointing that given the maximum surface winds from CMA at this time are ~33 m s^{-1}, although ExpTrec obviously improved over the other analyses, it is likely weaker than the true maximum winds at 3-km height level. To examine the vertical structure of the analyzed typhoon, the corresponding azimuthal mean tangential winds are also plotted in Figs. 4d-f. The vortex circulations in CTL (Fig. 4d) and ExpVr (Fig. 4e) are much weaker than that in ExpTrec (Fig. 4f), which shows a well-defined TC circulation structure with strong winds (>20 m s^{-1}) extending to about 8 km height while those in CTL and ExpVr are much shallower. Note that although the maximum wind speed at 3 km height in ExpVr reaches 27 m s^{-1}, the maximum mean tangential wind located at this level is only 16 m s^{-1} (Fig. 4e) owing to the asymmetric structure of vortex circulation (Fig. 4b). It is clear that the T-TREC-retrieved winds produce much more realistic wind structures of typhoon Meranti, especially in the inner core region, at this time when Meranti was of Category 1.

3.2. Impact on the track and intensity prediction

The verifications of track and intensity forecasts for CTL, ExpVr and ExpTrec are discussed in this subsection. Figure 5 shows the 18-h predicted typhoon track, track error, minimum sea-level pressure (MSLP) and maximum surface wind speed (MSW), verified against the best track data from CMA. During the period of landfall, Meranti moves northward with slight northwestward turn first, and then turns slightly northeastward about 3 hours after landfall. In both CTL and ExpVr, the predicted typhoon tracks turn unexpected northwestward in the first 3 hours and then bias eastward with the 18-hour mean errors being 50 km and 72 km, respectively. The predicted landfall times are all delayed with eastward bias of landfall locations. ExpVr actually moves slower and has a larger track error than CTL, presumably due to the strong asymmetric structures introduced into the vortex inner region by the V_r DA (Fig. 4b). In comparison, ExpTrec produces a closed inner core vortex circulation that is more axis-symmetric (Fig. 4c). With the improved IC, the predicted typhoon in ExpTrec shows a mostly northward track closer to the best track, although slower than observed before landfall, resulting in an 18-hour mean error of 32 km. Apparently, due to the limited spatial coverage and limited background error correlation scale, the radar data assimilation does not spread the impact very far from the data coverage regions, hence does not directly change the environment much. Still, the improvement to the typhoon structure by the T-TREC wind data is able to improve the track forecast (Fig. 5). One possible mechanism by which the inner core intensity and structure can affect TC track is the so-called 'beta gyre' effect [Holland et al. 1983]. Through planetary vorticity advection, a 'beta gyre' circulation form inducing cross vortex center flow that affects TC track.

The MSLP and MSW of three experiments are plotted along with the best track data in Fig. 5c and Fig. 5d. Clearly, CTL under-predicts the intensity in terms of both MSLP and MSW, mainly owing to the weak vortex in the IC. ExpVr is little different, with the 18-h mean MSLP (MSW) improvement over CTL [calculated as $\eta = 1 - \frac{\sum_{t=1}^{18} |ExpVr(t) - BEST(t)|}{\sum_{t=1}^{18} |CTL(t) - BEST(t)|}$, where BEST is for the best track data] of only 21.7% (18.1%). It indicates that assimilating V_r data only once at the given time in this case cannot improve the intensity forecasting much; local adjustments to the wind fields (Fig. 4b) bring limited impact to the forecast. ExpTrec shows a notable improvement in intensity forecast especially in terms of MSW. The 18-h mean MSLP (MSW) improvement over CTL [calculated as $\eta = 1 - \frac{\sum_{t=1}^{18} |ExpTrec(t) - BEST(t)|}{\sum_{t=1}^{18} |CTL(t) - BEST(t)|}$] is 43.0% (59.6%). It is noted that the analyzed MSLP and MSW in ExpTrec are nearly the same as those in CTL. For the MSLP, the limited increment is attributed to the weak multivariate covariance in background error covariance matrix of WRF 3DVAR between pressure and wind fields. For the MSW, although the winds at the higher levels are significantly enhanced (Fig. 4f), the surface wind increment is determined by the vertical spatial covariance and the surface wind speed are not sufficiently influenced by radar measurements (see also Fig. 4f), which at the location of maximum wind speed (Fig. 4c) is about 3 km above sea surface. Despite these obvious limitations with the WRF 3DVAR analysis, MSLP drops from 1001h Pa to 992 hPa during the first hour of forecast while MSW increases from 18 m s^{-1} to 27 m s^{-1} in 3 hours, clearly in response to the strong analyzed typhoon circulations at the lower-middle and upper levels. After the adjustment period of about 6 hours, the predicted MSW agrees with the best track data very well through the rest of forecasting hours (Fig. 5d). In comparison, the predicted MSLP at the time of the lowest best track MSLP of about 970 hPa at 1800 UTC (6 hour) only reached 988 hPa. The high MSLP forecast bias can be partly attributed to the mutual adjustment between pressure and analyzed wind fields after a single time analysis. The ineffectiveness of wind data in fully deepens a TC vortex in terms of MSLP has been found in earlier studies and the assimilation of additional reflectivity data tends to help within the ARPS system using the cloud analysis procedure [e.g., Zhao and Xue 2009].

It should also be pointed out that the best track MSLP estimation has large uncertainty. In this case, the lowest MSLP in the Japanese Meteorological Administration (JMA) best track data is actually only 985 hPa. To get some idea on the consistency between the best track MSLP and MSW, GBVTD wind retrieved which provide more accurate horizontal TC circulation with retrieval errors of only 2 m s^{-1} [Lee et al. 1999; Harasti et al. 2004] is performed using the radar V_r data; based on gradient wind balance with retrieved axis-symmetric circulation, the estimated MSLP is about 980 hPa [Zhao et al. 2012]. This suggests that the lowest CMA MSLP may be over-estimated.

To better represent the storm intensity, the azimuthal mean tangential winds and temperature anomalies at 1800 UTC are plotted in Figs. 6a-c. For further comparison, GBVTD-retrieved tangential winds are also displayed in Fig. 6d. Compared to CTL and ExpVr, ExpTrec shows much stronger tangential winds that extend from the surface to the upper levels; the outwardly-sloping isotachs in the inner core region conform to typical observed TC structures [e.g., Marks and Houze 1987] or simulation studies [e.g., Liu et al. 1997; 1999]. The predicted vortex in ExpTrec has a much smaller radius of maximum wind (RMW) of about 35 km and the maximum mean wind speed of 31 m s^{-1} found in the boundary layer is comparable to the 35 m s^{-1} GBVTD retrieval (Fig. 6d). Consistent with the stronger vortex circulation, the maximum temperature anomaly of 3.5 K (Fig. 6c) is much larger than those of 1 K in CTL (Fig. 6a) and 2.5 K in ExpVr (Fig. 6b). These results further confirm that ExpTrec predicts a typhoon whose wind structures are more consistent with GBVTD retrieval circulation while those in CTL and ExpVr do not possess the structures typical of a category 1 typhoon at this time.

To further examine the time trend of intensity predictions of three experiments, we plot in Fig. 7 the time-radius Hovmöller diagrams of azimuthal-averaged tangential wind speeds at 1 km height. Among the three experiments, only ExpTrec exhibits the correct intensity trend (c.f., Fig. 5d). In CTL (Fig. 7a), the typhoon remains weak throughout the forecast. Initially the storms are weak, with the peak tangential wind reaching only 12 m s^{-1} and broadly located around the radius of 120 km. During the entire forecast period, the maximum tangential winds do not change much and the RMW remains at close to 120 km radius until after 7 hours or so. Even after that, the stronger winds remain very broad (Fig. 7a). In ExpVr (Fig. 7b), with the help of V_r data, the peak tangential wind reaches 16 m s^{-1} and the RMW of about 60 km is much smaller than that in CTL at the initial time. The maximum tangential wind remains this level until about 8 hours (the landfalling time), however after that, the RMW shrinks with the tangential wind speed increased (Fig. 7b). It shows the unreasonable intensity trend in which the vortex circulation is intensified after landfall. As the predicted typhoon takes an eastern track closer to the coast with almost half of the vortex remaining over ocean in ExpVr (Fig. 5c), the intensity is over-predicted after 2000 UTC, because of slower decay of the vortex. In comparison, the peak tangential wind speed is about 24 m s^{-1} at 55 km radius at the IC time in ExpTrec (Fig. 7c). The RMW shrinks to about 40 km between 6 to 8 hours with the maximum wind increases to 32 m s^{-1} before landfall. After the landfall at 2000 UTC 9 September (8 hours from the IC time), the RMW increases gradually and the wind speed decreases below 18 m s^{-1} at the end of the forecast. This 'shrinking-expansion' process represents a correct trend of intensity change before and after landfall, that is consistent with the best track data shown in Fig. 5.

To estimate the thermal structure during the whole forecasting period, the time-height evolution of mean temperature anomalies (defined as the mean value of temperature anomalies within the radius of 150 km centered the typhoon's surface minimum pressure for simulations) for simulated storms in CTL, ExpVr and ExpTrec are plotted in Figure 8. There is no obvious warm core structure at all heights in CTL (Fig. 8a) suggesting the vortex structure is not well established during the forecast. For ExpVr, during the first 8 hours before landfall, the warm anomalies are weak similar with CTL. While, after 9 hours or so, the warm core appears at the level of about 7 km height. The delayed formation of warm core structure is consistent with the incorrect intensification after landfall in ExpVr (Fig. 7b). In comparison, for ExpTrec, the maximum warm anomalies take place in the middle level of about 8 km at the initial several hours of 1300 UTC to 1400 UTC (Fig. 8c) after the model adjustment. The layer of the warm core decreases to about 6 km after 9 hours as the storm declines due to the landfall. The peak anomaly in ExpTrec is much higher than that in ExpVr, suggesting the low predicted pressure (Fig. 5c) in ExpTrec. The results again indicate that the assimilation of T-TREC wind data at the given time is much more effective than assimilating available V_r data at the time.

3.3 Impact on the typhoon structure prediction

The composite radar reflectivity and 3-km height horizontal winds at 6, 12 and 18 hours from CTL, ExpVr and ExpTrec are plotted in Fig. 9, together with corresponding observed reflectivity fields (1st column).

At 1800 UTC, the 6-hour forecast time, reflectivity echoes are mainly found in the inner core region or are associated with the outer rainbands more on the south side (Fig. 9a). In CTL (Fig. 9b), the vortex circulation is not well organized in the inner core region while most of the predicted precipitation is in the northeastern quadrant unlike observed. Similar to CTL, ExpVr (Fig. 9c) over-predicts the reflectivity in the northern quadrant and misses the main precipitation structure in the inner core region. Besides, the predicted typhoon location has more southward bias in ExpVr. In comparison, precipitation structures in the inner core region are much strong in ExpTrec (Fig. 9d), so is the rainband extending south and southwestward on the south side. The eyewall structure is also evident. Imperfect aspects of the prediction include overly strong predicted reflectivity, and southerly displacement of the typhoon compared to observations; the former may be linked to deficiencies in the Lin microphysics scheme used while latter is linked to the too slow movement of the typhoon before landfall, as mentioned earlier. Still, the improvements over CTL and ExpVr are clear.

At 12 hours, Meranti has made landfall and the precipitation pattern becomes more asymmetric. The precipitation is mostly over land and the observed typhoon eye is now filled due to landfall. The weak storm in CTL (Fig. 9f) moves north-northeastward within the background flow, deviating from the observation, and typhoon structures are no longer clear. In ExpVr (Fig. 9g), the disorganized vortex structure also appears more south than the observed typhoon location the same as situation in the 6th forecast hour (Fig. 9c). However, the storm in ExpTrec still shows a much better organized vortex with reflectivity mostly found on the west side of the typhoon center (Fig. 9h), agreeing with observations (Fig. 9e). At 18 hours, the precipitation becomes even more asymmetric and weaker. The reflectivity structure nearly vanishes in CTL (Fig. 9j). While ExpVr (Fig. 9k) over-predict the reflectivity structure, indicating that the predicted typhoon is stronger than the observed typhoon during this time. The over-prediction is consistent with the incorrect intensity trend (Fig. 7b) shown before. In comparison, ExpTrec captures the distribution of strong echoes (Fig. 9l) in agreement with observations (Fig. 9i), although there is over-prediction in the reflectivity intensity which may be related to errors in the microphysics [Rogers et al. 2007].

To further quantify the reflectivity prediction skills, the Probability of Detection (POD) and False Alarm Rate (FAR) for CTL, ExpVr and ExpTrec at 1800 UTC, 0000 UTC and 0600 UTC are displayed in Figure 10. The PODs in ExpTrec for each valid time are much higher than those in CTL and ExpVr (Fig. 10a), suggesting that more observed reflectivity structures are successfully predicted in ExpTrec. Furthermore, ExpTrec also gets the lowest FAR scores at all three times among all three experiments (Fig. 10b), indicating that ExpTrec has a lower false alarm rate compared to the other two experiments. The predicted skills for CTL and ExpVr are similar in POD and FAR scores

(Figs. 10a, b). These quantitative scores again indicate that the assimilation of T-TREC winds is advantageous.

Overall, with improved IC, ExpTrec is able to capture the typhoon structures well during the entire 18-hourforecasting period. As Meranti in ExpTrec moves slower than the observation, the predicted typhoon eye is somewhat south of the observed center. Assimilating V_r data from a single radar for only one time in this case fails to reproduce the structure of typhoon inner core correctly, and actually the track forecasting even worse. Impacts are expected to be greater when more assimilation cycles and radars are used over a period of time [Xiao et al. 2005, Zhao and Xue 2009].

3.4. Impact on precipitation forecast

Figure 11 compares the 6-hour accumulated precipitation fields valid at 0000 and 0600 UTC, 10 September, respectively, from CTL, ExpVr and ExpTrec together with objective analyses of the automatic weather station rainfall measurements. During the landfall period, the observation (Fig. 11a) shows a band of strong precipitation along the coast of Fujian Province. Neither CTL (Fig. 11b) nor ExpVr (Fig. 11c) predicts this pattern or intensity, due to their eastward track bias and low intensity. On the contrary, ExpTrec (Fig. 11d) captures reasonably well the strong precipitation region near the coast. The precipitation distribution is more south than observation owing to its slower movement. After landfall, the main precipitation band moves north with the typhoon, producing an elongated region of high precipitation along 118.5 °E (Fig. 11e). CTL (Fig. 11f) has a northeastward bias of precipitation distribution with much smaller magnitude. While, ExpVr (Fig. 11g) represents a similar pattern as the observation except for the high precipitation located much more south. The precipitation of ExpTrec (Fig. 11h) compares with the observation much better in both distribution and intensity.

To quantify the precipitation forecast skills, equitable threat scores (ETS) and frequency bias scores of 12-hour accumulated precipitation valid at 0600 UTC 10 September against the rainfall observations are calculated and plotted for thresholds ranging from 0 mm to 150 mm in Figure 12. It is obvious that CTL has little skill in heavy rain prediction for thresholds above 50 mm (Fig. 12a). ExpVr has some improvement in the skill of heavy rain while the maximum ETS scores is only 0.22. Both of them also under-forecast the precipitation amounts for both weak and heavy rainfall (Fig. 12b). For all thresholds, ExpTrec has much higher ETS scores than other two experiments, with the maximum score being about 0.58 at about 20 mm threshold (Fig. 12a). ExpTrec also produces excellent frequency biases that are very close to 1 for more thresholds (Fig. 12b). The improvements in precipitation forecast are attributed to the improved intensity and structure forecasting.

4. Results of experiments with later analysis times

In this section, the results of the experiments with analysis times at 1400, 1600 and 1800 UTC are presented. For brevity, we focus on the predicted track and intensity in these experiments.

Figure 13 displays the observed and T-TREC-retrieved V_r at 3-km height at 1400, 1600 and 1800 UTC, 9 September. The T-TREC-retrieved V_r (Figs. 13b, d, f) shows quite similar patterns to observed V_r (Figs. 13a, c, e) at each time within the observed V_r coverage. At 1400 UTC, the observed V_r shows an incomplete velocity dipole pattern associated with typhoon inner core, while the T-TREC-retrieved V_r yields a more complete velocity dipole pattern. As the typhoon gets closer to the radar at 1600 and 1800 UTC, the observed V_r fully covers the typhoon inner core region (Figs. 13 c, e). However, the T-TREC-retrieved winds still have the advantage of being able to cover the complete TC circulation (Figs. 13d, f).

Figure 14 shows the track and intensity forecasts of all experiments (Table. 1). For all experiments that assimilate T-TREC winds, the mean predicted track, MSLP and MSW errors are similar in ExpTrec, ExpTrec14 and ExpTrec16. The mean MSLP (MSW) errors are 12.1 hPa (3.8 m s^{-1}), 12.4 hPa (3.7 m s^{-1}) and 12.3 hPa (3.1 m s^{-1}), respectively. However, since the assimilation time in ExpTrec18 is close to the landfall time of ~2000 UTC, and without the benefit of a longer model spin up, the predicted MSLP and MSW (Figs. 14c, d) in ExpTrec18 are much weaker than in earlier experiments before landfall and decline quickly further after landfall.

Among all the experiments that assimilate V_r data, the later assimilation times in ExpVr14 and ExpVr16 result in better track (Figs. 14a, b) and intensity forecasts (Figs. 14c, d) than in ExpVr. The mean track errors in ExpVr14 and ExpVr16 are 51 km and 49 km, respectively, smaller than the 72 km of ExpVr. The mean predicted MSLP (MSW) errors in ExpVr14 and ExpVr16 are 15.2 hPa (6.4 m s^{-1}) and 13.7 hPa (3.6 m s^{-1}), respectively, better than the 16.6 hPa (7.7 m s^{-1}) of ExpVr. The improved track and intensity forecasts can be attributed to the increasingly larger V_r coverage as Meranti moves closer to the radar (Figs. 13a, c). It is worth pointing out that, as TC approaches the coastline, the performance of V_r assimilation in ExpVr16 and ExpVr18 becomes close to the T-TREC assimilation in ExpTrec16 and ExpTrec18. The mean MSLP (MSW) errors are 13.7 hPa (3.6 m s^{-1}) and 13.5 hPa (5.5 m s^{-1}) in ExpVr16 and ExpVr18, in comparison to the 12.3 hPa (3.1 m s^{-1}) and 13 hPa (5.3 m s^{-1}) in ExpTrec16 and ExpTrec18. Yet, the assimilation of T-TREC data at 1600 UTC and 1800 UTC still maintains a slight advantage.

Overall, except for the assimilation at 1800 UTC which is very close to landfall, the assimilation of T-TREC data 8 to 4 hours before landfall, shows consistently positive impacts on the forecast of typhoon Meranti. For V_r data, later analysis times result in larger positive impacts but the forecasts are generally poorer than the corresponding T-TREC assimilation experiments. The difference between V_r and T-TREC assimilations is largest at the earliest time when T-TREC retrieval can be successfully performed. The much improved forecast at a longer lead time with the T-TREC DA is especially valuable for real time decision making.

5. Summary and conclusions

An extended TREC technique, called T-TREC, was developed recently for retrieving wind circulations in TCs from single Doppler radar reflectivity (Z) and radial velocity (V_r) data from two consecutive times. This study explores, for the first time, the assimilation of T-TREC-retrieved wind data for the analysis and prediction of a TC. The WRF 3DVAR is used for the data assimilation while the landfalling typhoon Meranti (2010) near southeastern coast of China is chosen as the test case. The main conclusions are summarized as follows.

A single-time analysis at 1200 UTC, 9 September is first performed when the center of Meranti was in the full coverage of reflectivity data (which has a 460 km range from radar) of the Xiamen radar in Fujian Province, but the radial velocity only provides partial coverage of typhoon circulation and misses much of the inner core structure. Results show that the assimilation of T-TREC-retrieved wind data improves the inner core circulation of typhoon significantly, while the assimilation of V_r data only makes differences within the Doppler coverage at the given analysis time. The asymmetric vortex structure brought by the single-time assimilation of V_r data fails to reproduce the reasonable predicted typhoon throughout the entire forecasting period. The track forecast is actually even worse and the intensity forecast has incorrect trend especially after landfall. On the contrary, the effectiveness of the T-TREC-retrieved wind data is associated with the large spatial coverage of reflectivity data used for the retrieval and the complete typhoon inner core circulation that can be effectively represented by the T-TREC retrieval. The resulting improved typhoon intensity and structure leads to better track, intensity and structure predictions throughout the 18 hours of forecast. The predicted intensity shows a correct trend also. Benefiting from the improved track and structure forecasting, the heavy rain at coastal Fujian province of China is reproduced well in term of both intensity and distribution. Excellent precipitation ETS scores and frequency bias are obtained. The results indicates the efficacy of assimilating T-TREC-retrieved winds for TC initiations when such data can be retrieved from reflectivity data with much farther offshore reach than radial velocity data with typical operational weather radars. Additional experiments with later assimilation times and closer radar distances show that the assimilation of T-TREC winds consistently outperforms V_r assimilation, although the difference becomes smaller as the V_r coverage improves with time.

Because the T-TREC retrieval procedure is computationally rather efficient, the T-TREC-retrieved winds can be easily used for operational forecasting. The use of T-TREC winds can also help extend the utilization of radar data by several hours for a landfalling TC, because of the typical farther reach of the reflectivity data used for the retrieval, thereby benefiting advanced typhoon warning. Although conclusions drawn within this paper are based on a single landfalling typhoon, we have applied the same approach to typhoon Chanthu (2010) and all the results are consistent with the findings here. In the future, we will test the procedure with more cases. At the same time, we are also examining the impacts of V_r versus T-TREC winds by assimilating the data using the more advanced ensemble Kalman filter method for another typhoon [Wang et al. 2013]; similarly encouraging results are obtained.

A few other issues will require further research. When the typhoon gets closer to the coast, it may be covered by several coast radars. Direct assimilation of V_r data from multiple Doppler radars may become more effective while the relative advantage of using T-TREC-retrieved winds may decrease. It is also possible to assimilate both V_r and T-TREC retrievals at the same time, and the data can be assimilated through continuous cycles. It would also be interesting to compare the assimilation of T-TREC winds and the assimilation of GBVTD retrieval winds [Zhao et al. 2011] when both are available. The relative impacts of assimilating each type of data alone or in combination through varied assimilation procedure are worthy topics for future research.

Acknowledgments: This work was primarily supported by the Social Common wealth Research Program (GYHY201006007), the National Fundamental Research 973 Program of China (2009CB421502 and 2013CB430100), and the Chinese Natural Science Foundation (grants 41105035, 40975011 and 40921160381). We are grateful to the High Performance Computing Center of Nanjing University for doing the numerical calculations in this paper on its IBM Blade cluster system. We also thank the three anonymous reviewers who provided valuable suggestions for improving our manuscript.

References

Barker, D. M., W. Huang, Y.-R. Guo, A. J. Bourgeois, and Q. N. Xiao (2004), A three-dimensional variational data assimilation system for MM5: Implementation and initial results, *Mon. Weather Rev.*, *132*, 897–914.

Brown, R. A., and V. T. Wood (1983), Improved severe storm warning using Doppler radar, *National Weather Digest*, *8*(3), 19-27.

Chen, F., and J. Dudhia (2001), Coupling an advanced land-surface/ hydrology model with the Penn State/ NCAR MM5 modeling system. Part I: Model description and implementation, *Mon. Weather Rev.*, *129*, 569–585.

Chen, S.-H., and W.-Y. Sun (2002), A one-dimensional time dependent cloud model, *J. Meteorol. Soc. Japan*, *80*, 99–118.

Chou, K.-H., C.-C. Wu, P.-H. Lin, S. D. Aberson, M. Weissmann, F. Harnisch, and T. Nakazawa (2011), The impact of dropwindsonde observations on typhoon track forecasts in DOTSTAR and T-PARC, *Mon. Weather Rev.*, *139*, 1728–1743.

Dong, J., and M. Xue (2012), Assimilation of radial velocity and reflectivity data from coastal WSR-88D radars using ensemble Kalman filter for the analysis and forecast of landfalling hurricane Ike (2008), *Q. J. R. Meteorol. Soc.*, DOI: 10.1002/qj.1970.

Du, N., M. Xue, K. Zhao, and J. Min (2012), Impact of assimilating airborne Doppler radar velocity data using the ARPS 3DVAR on the analysis and prediction of hurricane Ike (2008). *J. Geophy. Res.*, *117*, D18113.

Dudhia, J. (1989), Numerical study of convection observed during the winter monsoon experiment using a mesoscale two-dimensional model, *J. Atmos. Sci.*, *46*, 3077–3107.

Hamill, T. M., J. S. Whitaker, M. Fiorino, and S. G. Benjamin (2011), Global Ensemble Predictions of 2009's Tropical Cyclones Initialized with an Ensemble Kalman Filter, *Mon. Weather Rev.*, *139*, 668–688.

Harasti, P. R., C. J. McAdie, P. P. Dodge, W. C. Lee, J. Tuttle, S.T. Murillo, and F. D. Marks (2004), Real-time implementation of single-Doppler radar analysis methods for tropical cyclones: Algorithm improvements and use with WSR-88D display data, *Weather Forecast.*, *19,* 219-239.

Holland, G. J. (1983), Tropical cyclone motion: Environmental interaction plus a beta effect, *J. Atmos. Sci*., *40*, 328–342.

Houze, R. A., Jr., S. S. Chen, B. F. Smull, W. C. Lee, and M. M. Bell (2007), Hurricane intensity and eyewall replacement, *Science*, *315*, 1235-1239.

Kain, J. S., and J. M. Fritsch (1990), A one-dimensional entraining/ detraining plume model and its application in convective parameterization, *J. Atmos. Sci.*, *47*, 2784–2802.

Kain, J. S. (2004) The Kain-Fritsch convective parameterization: An update. *J. Appl. Meteorol. Climatol.*, *43*, 170–181.

Lee, W. C., B. J. D. Jou, P. L. Chang, and S. M. Deng (1999), Tropical cyclone kinematic structure retrieved from Single-Doppler radar observations. Part I: Interpretation of Doppler velocity patterns and the GBVTD technique, *Mon. Weather Rev.*, *127*, 2419-2439.

Li, Y., X. Wang, and M. Xue (2012), Assimilation of radar radial velocity data with the WRF ensemble-3DVAR hybrid system for the prediction of hurricane Ike (2008), *Mon. Weather Rev.*, *140***,** 3507-3524.

Lin, Y.-L., R. D. Farley, and H. D. Orville (1983), Bulk parameterization of the snow field in a cloud model, *J. Appl. Meteorol. Climatol.*, *22*, 1065**–**1092.

Liu, Y., D.-L. Zhang, and M. K. Yau (1997), A multiscale numerical study of Hurricane Andrew (1992). Part I: An explicit simulation, *Mon. Weather Rev.*, *125***,** 3073–3093.

Liu, Y., D.-L. Zhang, and M. K. Yau (1999), A multiscale numerical study of hurricane Andrew (1992). Part II: Kinematics and inner-core structures, *Mon. Weather Rev.*, *127*, 2597-2616.

Marks, F. D, and R. A. Houze Jr. (1987), Inner core structure of Hurricane Alicia from airborne Doppler-radar observations. *J. Atmos. Sci., 44***,** 1296–1317.

Mlawer, E. J., S. J. Taubman, P. D. Brown, and M. J. Iacono (1997), Radiative transfer for inhomogeneous atmospheres: RRTM, a validated correlated-k model for the longwave. *J. Geophys. Res*., 102, 16 663–16 682.

Monin, A. S., A. M. Obukhov, Basic laws of turbulent mixing in the ground layer of the atmosphere, in Russian, *Tr. Geofiz. Inst. Akad. Nauk SSR*, *24151*,163–187, 1954.

Noh, Y., W. G. Cheon, S.-Y. Hong, and S. Raasch (2003), Improvement of the K-profile model for the planetary boundary layer based on large eddy simulation data, *Boundary Layer Meteorol., 107*, 401–427.

Oye, R., C. Mueller, and C. Smith (1995), Software for radar data translation, visualization, editing, and interpolation, in *27th Conference on Radar Meteorology*, pp. 359–361, Am. Meteorol. Soc., Boston, Mass.

Pu, Z., X. Li, C. Velden, S. Aberson, and W. T. Liu (2008), Impact of aircraft dropsonde and satellite wind data on the numerical simulation of two landfalling tropical storms during the Tropical Cloud Systems and Processes Experiment, *Weather Forecast.*, *23*, 62–79.

Pu, Z., X. Li, and J. Sun (2009), Impact of airborne Doppler radar data assimilation on the numerical simulation of intensity changes of Hurricane Dennis near a landfall, *J. Atmos. Sci.*, *66*, 3351–3365.

Rappaport E. N., J. L. Franklin, L. A. Avila, S. R. Baig, J. L. Beven, E. S. Blake, C. A. Burr, J.-G. Jiing, C. A. Juckins, R. D. Knabb, C. W. Landsea, M. Mainelli, M. Mayfield, C. J. Mcadie, R. J. Pasch, C. Sisko, S. R. Stewart, and A. N. Tribble, (2009), Advances and Challenges at the National Hurricane Center. *Weather Forecast.*, *24*, 395-419.

Rogers, R. F., M. L. Black, S. S. Chen, and R. A. Black (2007), An evaluation of microphysics fields from mesoscale model simulations of tropical cyclones. Part I: Comparisons with observations. *J. Atmos. Sci.*, *64*, 1811–1834.

Roux, F., and F. D. Marks (1996) Extended velocity track display (EVTD): An improved processing method for Doppler radar observations. Part I: Kinematics, *Mon. Weather Rev.*, *123*, 2611-2639.

Skamarock, W. C., J. B. Klemp, J. Dudhia, D. O. Gill, D. M. Barker, M. G. Duda, X.-Y. Huang, W. Wang, and J. G. Powers (2008), Description of the Advanced

Research WRF version 4, Rep. NCAR/TN-475++STR, Natl. Cent. for Atmos. Res., Boulder, Colo.

Tuttle, J., and R. Gall (1999), A single-radar technique for estimating the winds in tropical cyclones, *Bull. Am. Meteorol. Soc.*, *80*, 653-668.

Wang, M. J., K. Zhao, and D. Wu (2011), The T-TREC technique for retrieving the winds of landfalling typhoons in China, *Acta Meteorol. Sin*, *25*, 91-103.

Wang, M., M. Xue, K. Zhao, and J. Dong (2013), Assimilation of T-TREC-retrieved winds from single-Doppler radar with an EnKF for the forecast of Typhoon Jangmi (2008), *Mon. Weather Rev.*, Being submitted.

Weng Y., and F. Zhang (2012), Assimilating Airborne Doppler Radar Observations with an Ensemble Kalman Filter for Convection-Permitting Hurricane Initialization and Prediction: Katrina (2005), *Mon. Weather Rev.*,*140*, 841-859.

Xiao, Q., Y.-H. Kuo, J. Sun, W.-C. Lee, E. Lim, Y.-R. Guo, and D. M. Barker (2005), Assimilation of Doppler radar observations with a regional 3DVAR system: Impact of Doppler velocities on forecasts of a heavy rainfall case, *J. Appl. Meteorol. Climatol.*, *44*, 768–788.

Xiao, Q., and J. Sun (2007), Multiple-Radar Data Assimilation and Short-Range Quantitative Precipitation Forecasting of a Squall Line Observed during IHOP_2002, *Mon. Weather Rev.*, *135*, 3381–3404.

Xiao Q, L. Chen, and X. Zhang (2009a), Evaluations of BDA scheme using the Advanced Research WRF (ARW) model, *J. Appl. Meteorol. Climatol.*, *48,* 680-689.

Xiao, Q., X. Zhang, C. A. Davis, J. Tuttle, G. J. Holland, and P. J. Fitzpatrick (2009b), Experiments of hurricane initialization with airborne Doppler radar data for the advanced research hurricane WRF (AHW) model, *Mon. Weather Rev.*, *137*, 2758– 2777.

Xue, M., D. H. Wang, J. D. Gao, K. Brewster, and K. K. Droegemeier (2003), The Advanced Regional Prediction System (ARPS), storm-scale numerical weather prediction and data assimilation, *Meteorol. Atmos. Phys.*, *82*(1-4), 139-170.

Zhang F., Y. Weng, J. A. Sippel, Z. Meng, and C. H. Bishop (2009), Cloud-resolving hurricane initialization and prediction through assimilation of Doppler radar observations with an ensemble Kalman filter, *Mon. Weather Rev., 137*, 2105-2125.

Zhao, K., and M. Xue (2009), Assimilation of coastal Doppler radar data with the ARPS 3DVAR and cloud analysis for the prediction of Hurricane Ike (2008), *Geophys. Res. Lett.*, 36, doi:10.1029/2009GL038658.

Zhao, K., M. Xue, and W.-C. Lee (2011), Assimilation of GBVTD-retrieved winds from single-Doppler radar for short-term forecasting of super typhoon Saomai (0608) at Landfall, *Q. J. R. Meteorol. Soc.*, *138*, 1055–1071.

Zhao, K., X. Li, M. Xue, B. J.-D. Jou, and W.-C. Lee (2012), Short-term forecasting through intermittent assimilation of data from Taiwan and mainland China coastal radars for Typhoon Meranti (2010) at landfall, *J. Geophys. Res.*, 117, D06108, doi:10.1029/2011JD017109.

Zou X., and Q. Xiao (2000), Studies on the initialization and simulation of a mature hurricane using a variational bogus data assimilation scheme, *J. Atmos. Sci. 57*, 836-860.

List of figures

Fig. 1. The domain for radar data coverage at 1200 UTC, 9 September, with the CMA best track locations of Typhoon Meranti marked with 6-h interval from 1200 UTC, 9 September to 0600 UTC, 10 September, 2010. The V_r data (color shaded, m s^{-1}) is shown in (a), the Z data (color shaded, dBZ) and the T-TREC-retrieved wind data (vectors) are shown in (b), respectively at 3 km height. Small and large circles in both (a) and (b) are the 230-km range ring of V_r data and 460-km range ring of Z data.

Fig. 2. A schematic diagram of the T-TREC method. OM and OR indicate the maximum searching distance and the referenced searching distance along the azimuth direction, respectively. $\overline{AB}$ is twice as long as the radial referenced searching distance. The hatching indicates the area with larger weight. (reproduced from Wang et al. 2011)

Fig. 3. Percent cumulative histogram of the difference between measured Doppler radial velocities and the retrieved radial component of T-TREC winds for typhoon Meranti. N represents the total number of available radial velocities. R and E represent the correlation coefficient and the mean difference, respectively.

Fig. 4. The analyzed horizontal wind vectors and speed (color shaded, m s^{-1}) at 3 km height after one time analysis at 1200 UTC for (a) CTL initialized from GFS analysis at 1200 UTC, (b) the analysis from ExpVr using V_r data, and (c) the analysis from ExpTrec using T-TREC-retrieved wind data. Also shown are the analyzed azimuthal winds at the same time from experiments (d) CTL, (e) ExpVr, and (f) ExpTrec. Black dots in both (a), (b) and (c) are the typhoon centers from CMA best track.

Fig. 5. The 18-h predicted (a) tracks, (b) track errors, (c) MSLP (hPa), and (d) MSW (m s^{-1}), for typhoon Meranti (2010), from 1200 UTC, 9 September to 0600 UTC, 10

September 2010. The numbers in (b) represent the mean track errors over the 18 hours period. Best track data are shown in black and 3 hours apart in (a).

Fig. 6. Azimuthal mean tangential winds (color shaded, m s^{-1}) and temperature deviation (solid isolines) of the 6-hour forecast valid at 1800 UTC for experiments (a) CTL, (b) ExpVr, and (c) ExpTrec, as compared with the (d) GBVTD-derived azimuthal mean tangential wind.

Fig. 7. Time-radius Hovmöller diagrams of azimuthal-averaged tangential wind (m s^{-1}) at 1 km height from three experiments: (a) CTL, (b) ExpVr and (c) ExpTrec. The thick line denotes the RMW at the same height.

Fig. 8. Time-height diagrams of mean temperature anomalies from three experiments: (a) CTL, (b) ExpVr and (c) ExpTrec. The average is computed within the radius of 150 km centered at the typhoon’s surface minimum pressure for simulations.

Fig. 9. Composite reflectivity (color shaded) and wind vectors at 3 km height predicted by experiments CTL (2nd column), ExpVr (3rd column) and ExpTrec (4th column), as compared to observed composite reflectivity (1st column). The corresponding times are 1800 UTC (6h), 9 September, and 0000 UTC (12h), 0600 UTC (18h), 10 September.

Fig. 10. (a) Probability of detection and (b) False alarm rate for the predicted composite reflectivity from CTL, ExpVr and ExpTrec at 1800 UTC 9 September, 0000 UTC 10 September and 0600 UTC 10 September, verifed against the observed composite reflctivity.

Fig. 11. Six-hour accumulated precipitation (mm) valid at 0000 UTC (1^{st} row) and 0600 UTC (2^{nd} row), on 10 September 2010 fromautomatic weather station hourly

observations (1st column), CTL (2nd column), ExpVr (3rd column), and ExpTrec (4th column).

Fig. 12. (a) Equitable threat scores and (b) bias scores of the 12-h accumulated precipitation forecast valid at 0600 UTC 10 September from CTL, ExpVr and ExpTrec verified against the automatic weather station obervations.

Fig. 13. (a, c, e) Observed radial velocity and (b, d, f) the radial velocity calculated from T-TREC winds at 3 km height at 1400 UTC (1st row), 1600 UTC (2nd row) and 1800 UTC (3rd row), 9 September 2010. '+' denotes the center of vortex.

Fig. 14. The predicted (a) tracks, (b) track errors, (c) MSLP (hPa), and (d) MSW (m s^{-1}), for experiments ExpVr, ExpVr14, ExpVr16, ExpVr18, ExpTrec, ExpTrec14, ExpTrec16 and ExpTrec18. The numbers in (b), (c) and (d) represent the mean track errors, mean MSLP errors and mean MSW errors, respectively. The vertical dashed line in (c) and (d) represent the landfalling time for typhoon Meranti (2010).

Table 1. Description of experiments

Experiments	Description
CTL	No radar data assimilation
ExpVr	Assimilating radial velocity once at 1200 UTC, 9 September
ExpTrec	Assimilating T-TREC winds once at 1200 UTC, 9 September
ExpVr14	Same as ExpVr, but assimilating radial velocity at 1400 UTC
ExpTrec14	Same as ExpTrec, but assimilating T-TREC winds at 1400 UTC
ExpVr16	Same as ExpVr, but assimilating radial velocity at 1600 UTC
ExpTrec16	Same as ExpTrec, but assimilating T-TREC winds at 1600 UTC
ExpVr18	Same as ExpVr, but assimilating radial velocity at 1800 UTC
ExpTrec18	Same as ExpTrec, but assimilating T-TREC winds at 1800 UTC

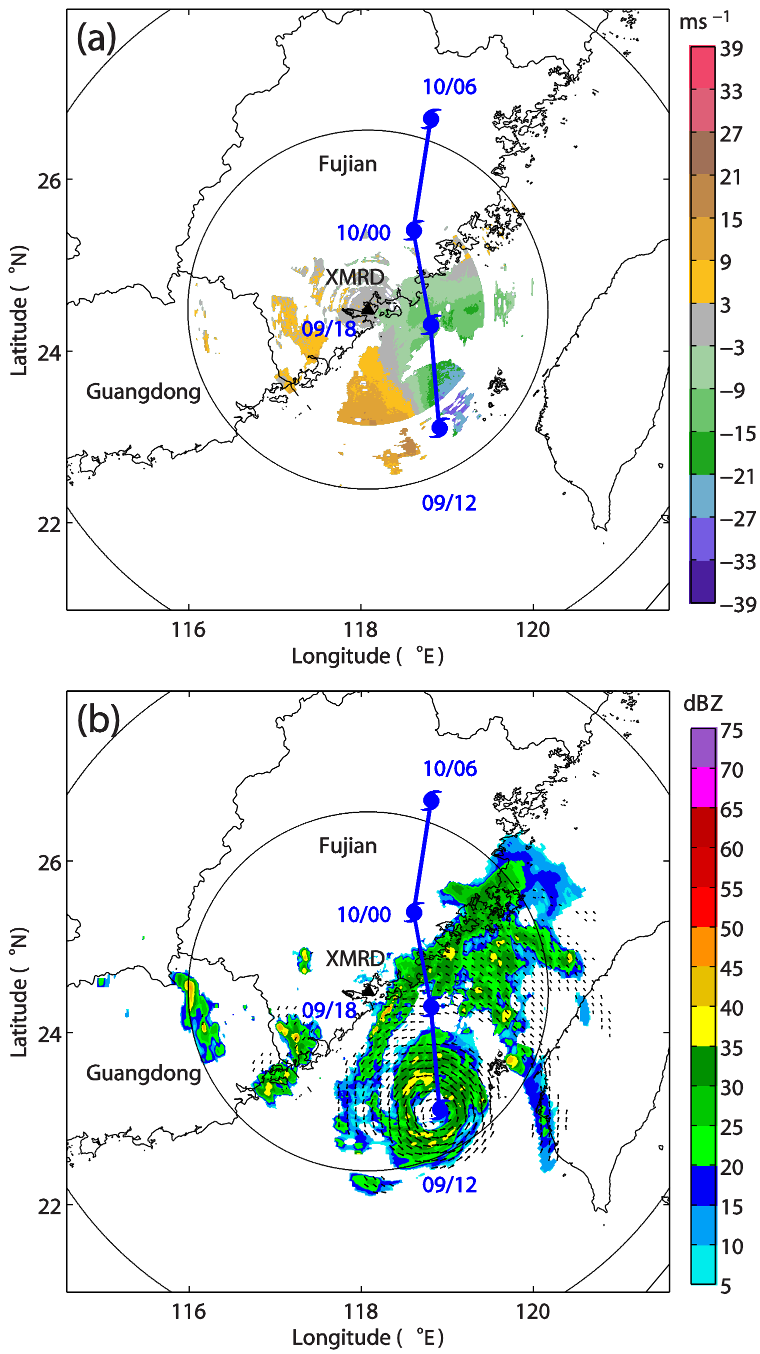

Fig. 1. The domain for radar data coverage at 1200 UTC, 9 September, with the CMA best track locations of Typhoon Meranti marked with 6-h interval from 1200 UTC, 9 September to 0600 UTC, 10 September, 2010. The V_r data (color shaded, m s^{-1}) is shown in (a), the Z data (color shaded, dBZ) and the T-TREC-retrieved wind data (vectors) are shown in (b), respectively at 3 km height. Small and large circles in both (a) and (b) are the 230-km range ring of V_r data and 460-km range ring of Z data.

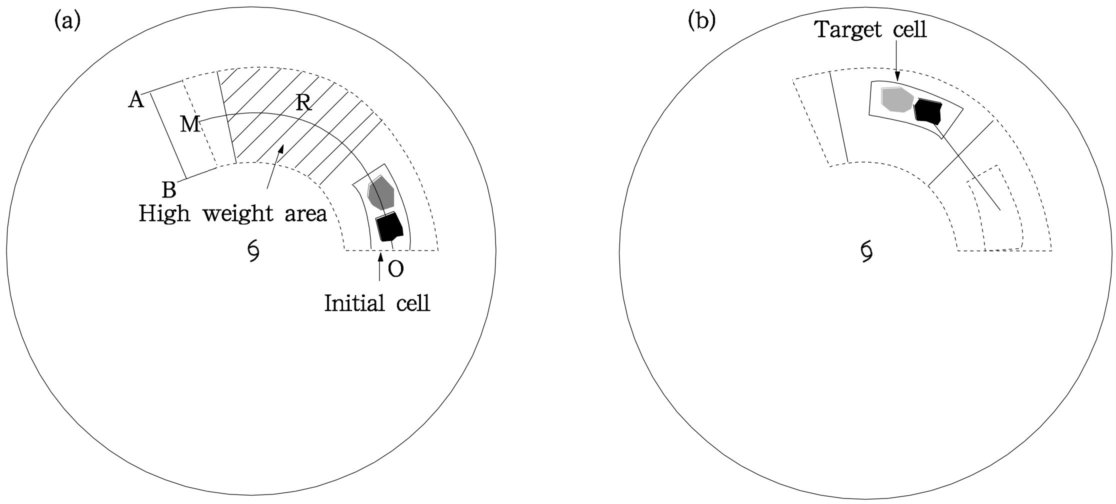

Fig. 2. A schematic diagram of the T-TREC method. OM and OR indicate the maximum searching distance and the referenced searching distance along the azimuth direction, respectively. $\overline{AB}$ is twice as long as the radial referenced searching distance. The hatching indicates the area with larger weight. (reproduced from Wang et al. 2011)

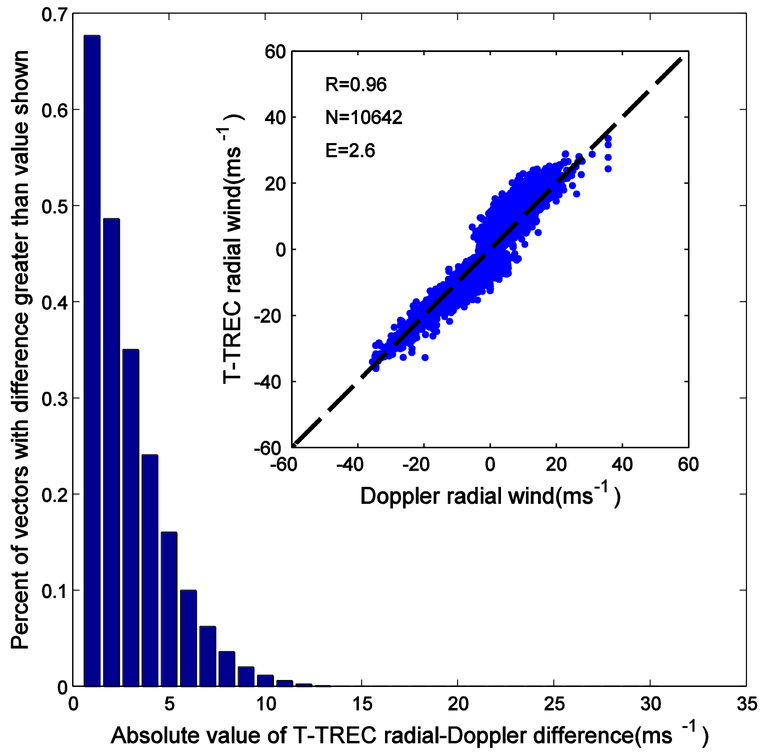

Fig. 3. Percent cumulative histogram of the difference between measured Doppler radial velocities and the retrieved radial component of T-TREC winds for typhoon Meranti. N represents the total number of available radial velocities. R and E represent the correlation coefficient and the mean difference, respectively.

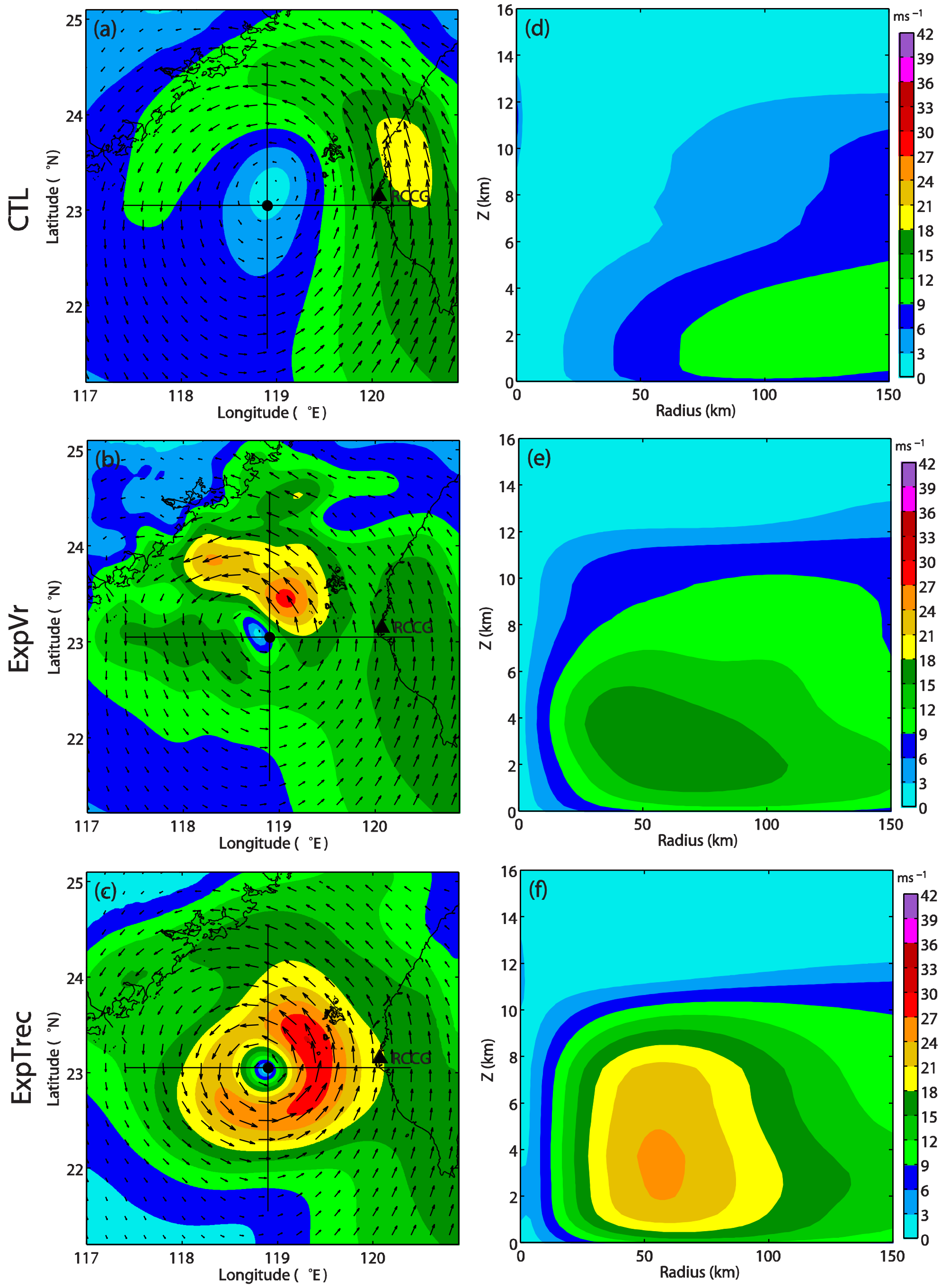

Fig. 4. The analyzed horizontal wind vectors and speed (color shaded, m s^{-1}) at 3 km height after one time analysis at 1200 UTC for (a) CTL initialized from GFS analysis at 1200 UTC, (b) the analysis from ExpVr using V_r data, and (c) the analysis from ExpTrec using T-TREC-retrieved wind data. Also shown are the analyzed azimuthal winds at the same time from experiments (d) CTL, (e) ExpVr, and (f) ExpTrec. Black dots in both (a), (b) and (c) are the typhoon centers from CMA best track.

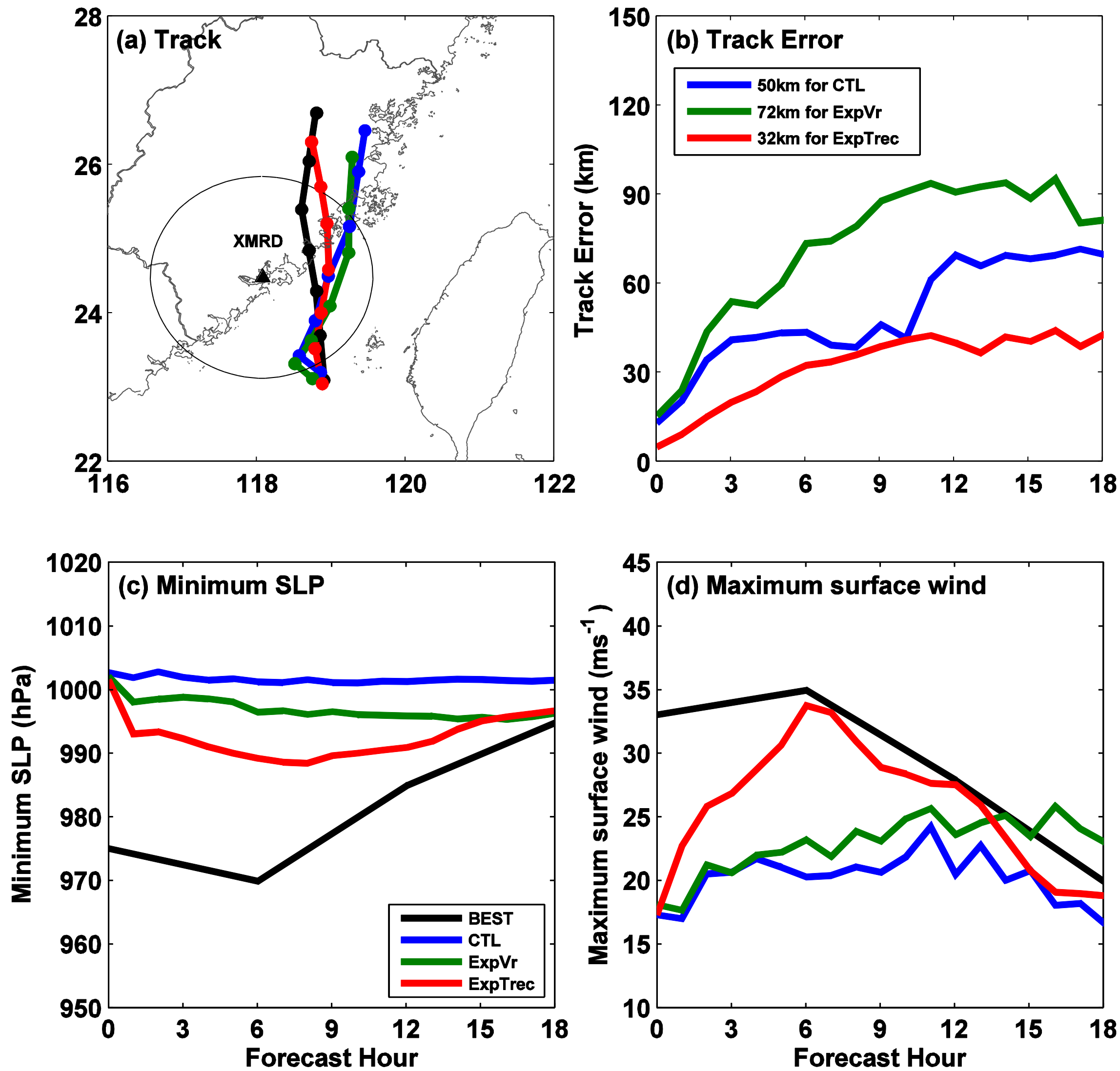

Fig. 5. The 18-h predicted (a) tracks, (b) track errors, (c) MSLP (hPa), and (d) MSW (m s^{-1}), for typhoon Meranti (2010), from 1200 UTC, 9 September to 0600 UTC, 10 September 2010. The numbers in (b) represent the mean track errors over the 18 hours period. Best track data are shown in black and 3 hours apart in (a).

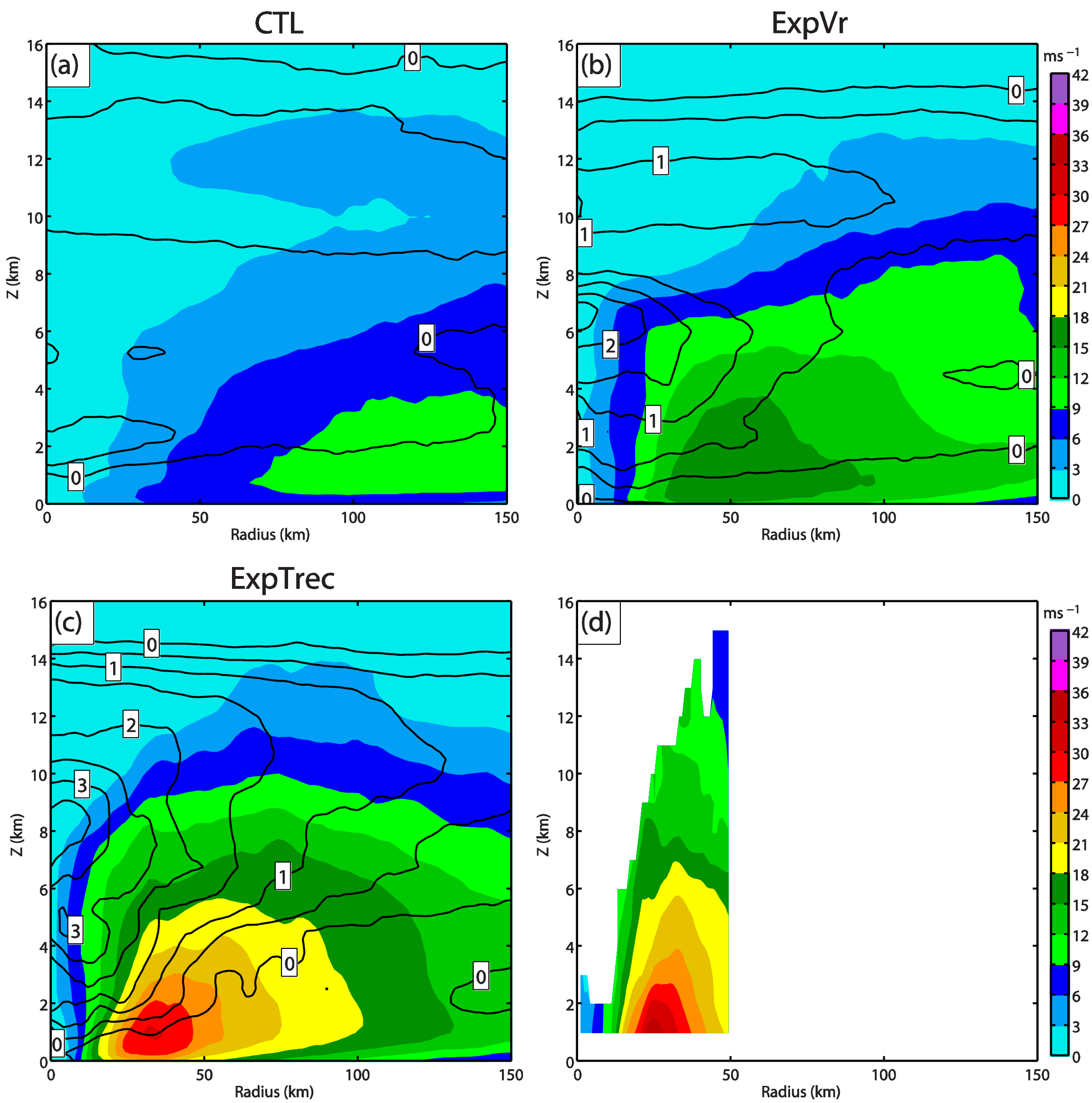

Fig. 6.Azimuthal mean tangential winds (color shaded, m s^{-1}) and temperature deviation (solid isolines) of the 6-hour forecast valid at 1800 UTC for experiments (a) CTL, (b) ExpVr, and (c) ExpTrec, as compared with the (d) GBVTD-derived azimuthal mean tangential wind.

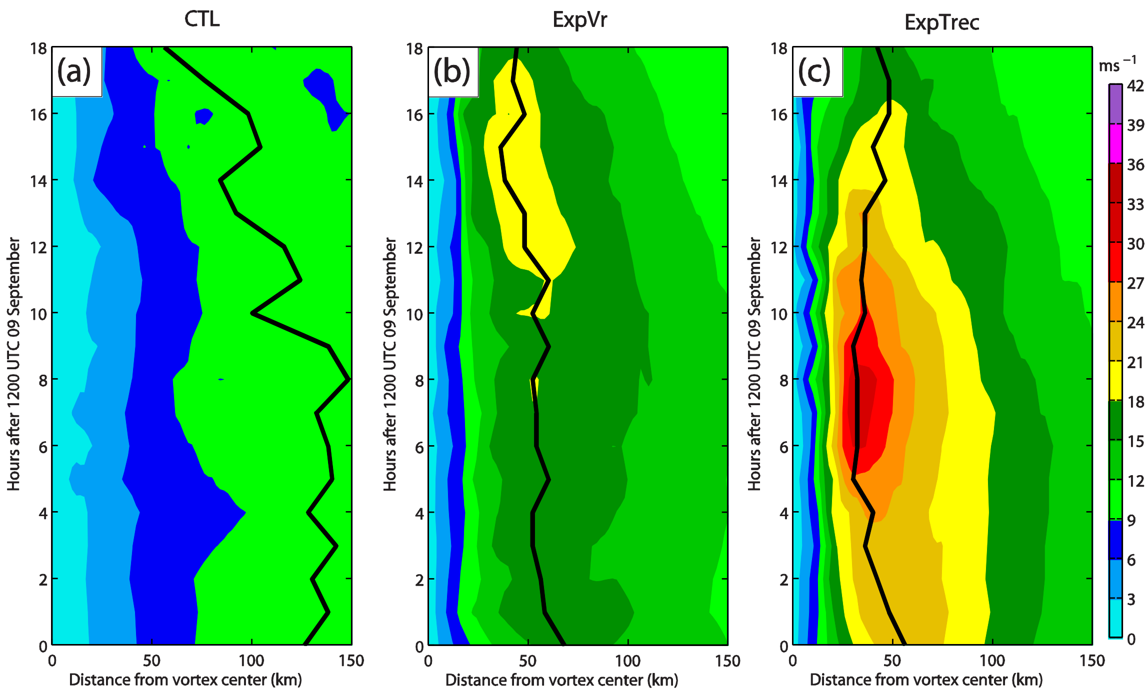

Fig. 7. Time-radius Hovmӧller diagrams of azimuthal-averaged tangential wind (m s^{-1}) at 1 km height from three experiments: (a) CTL, (b) ExpVr and (c) ExpTrec. The thick line denotes the RMW at the same height.

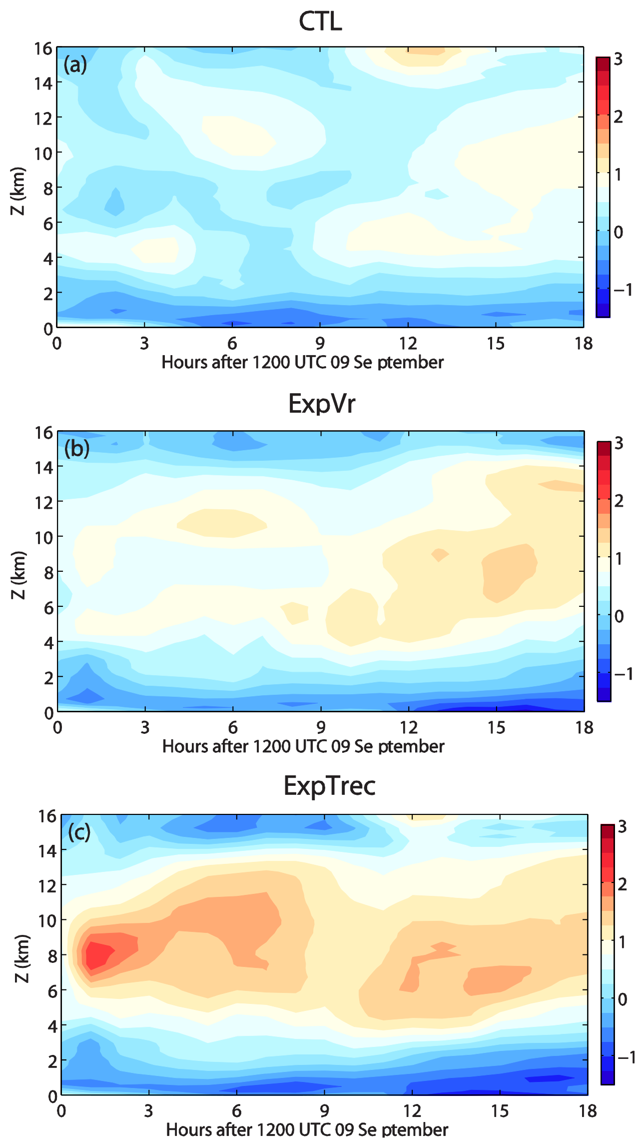

Fig. 8. Time-height diagrams of mean temperature anomalies from three experiments: (a) CTL, (b) ExpVr and (c) ExpTrec. The average is computed within the radius of 150 km centered at the typhoon's surface minimum pressure for simulations.

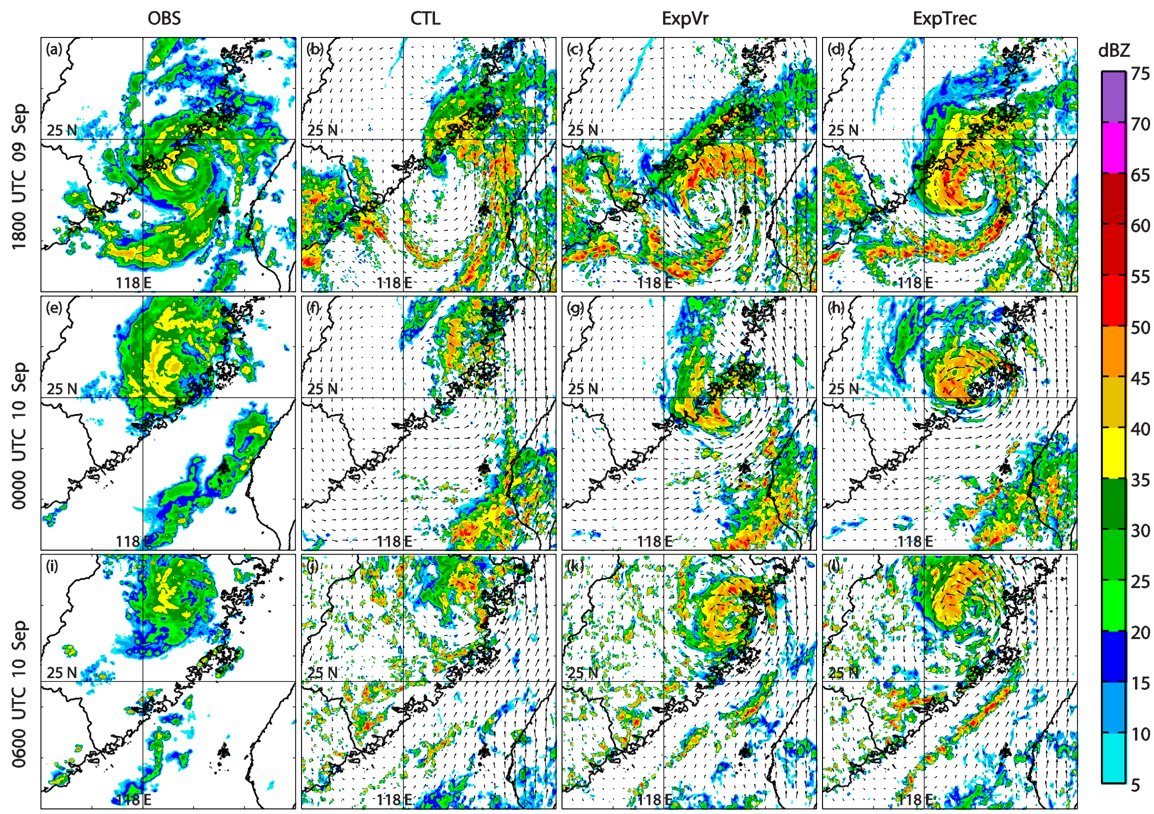

Fig. 9. Composite reflectivity (color shaded) and wind vectors at 3 km height predicted by experiments CTL (2nd column), ExpVr (3rd column) and ExpTrec (4th column), as compared to observed composite reflectivity (1st column). The corresponding times are 1800 UTC (6h), 9 September, and 0000 UTC (12h), 0600 UTC (18h), 10 September.

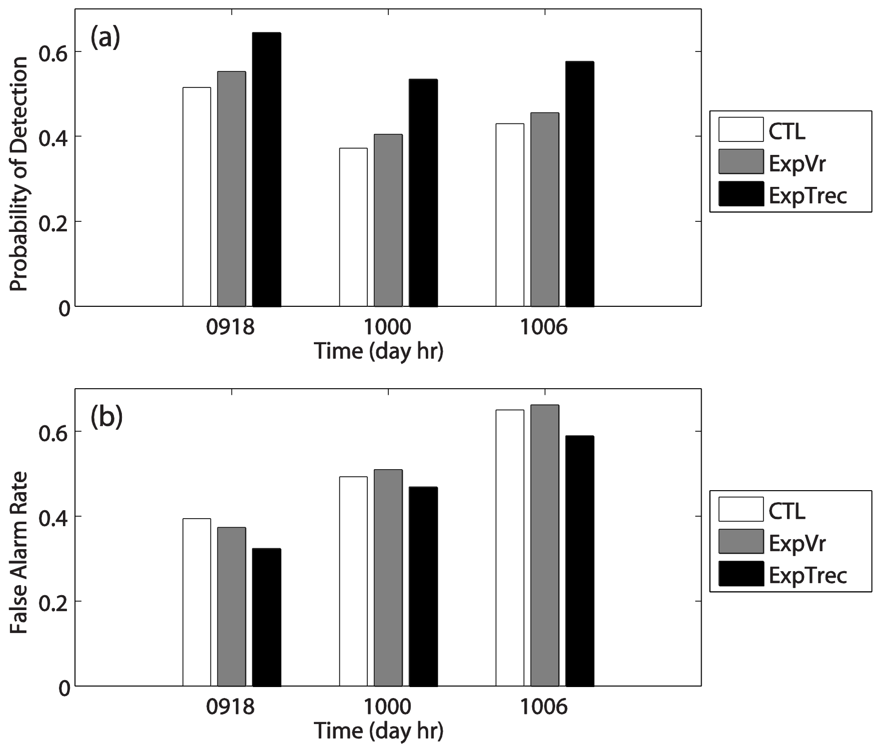

Fig. 10. (a) Probability of detection and (b) False alarm rate for the predicted composite reflectivity from CTL, ExpVr and ExpTrec at 1800 UTC 9 September, 0000 UTC 10 September and 0600 UTC 10 September, verifed against the observed composite reflctivity.

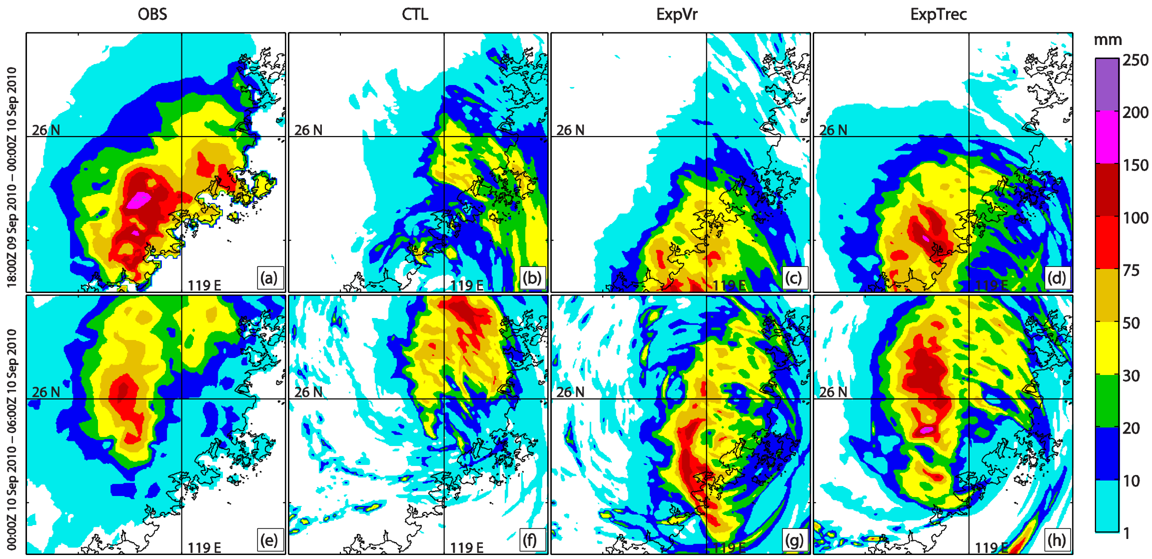

Fig. 11. Six-hour accumulated precipitation (mm) valid at 0000 UTC (1st row) and 0600 UTC (2nd row), on 10 September 2010 fromautomatic weather station hourly observations (1st column), CTL (2nd column), ExpVr (3rd column), and ExpTrec (4th column).

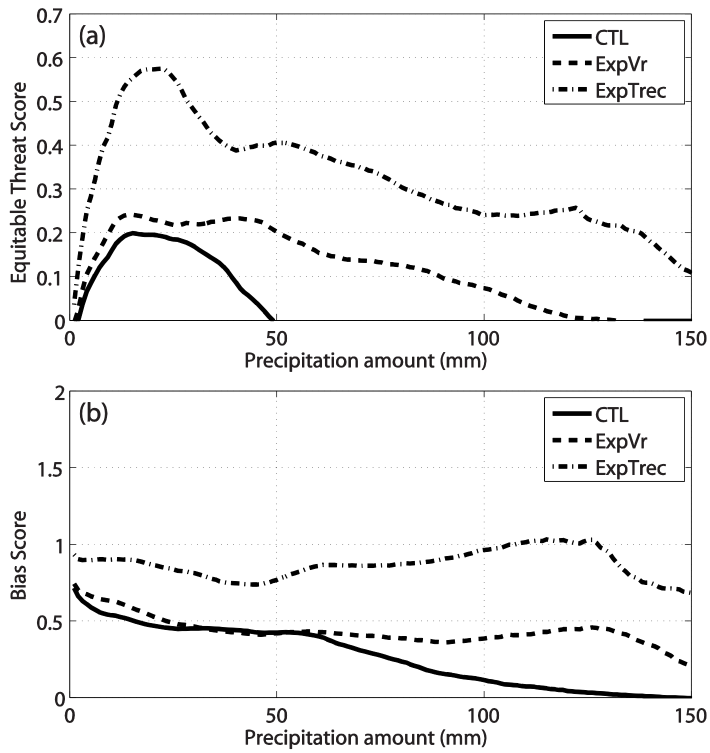

Fig. 12. (a) Equitable threat scores and (b) bias scores of the 12-h accumulated precipitation forecast valid at 0600 UTC 10 September from CTL, ExpVr and ExpTrec verified against the automatic weather station obervations.

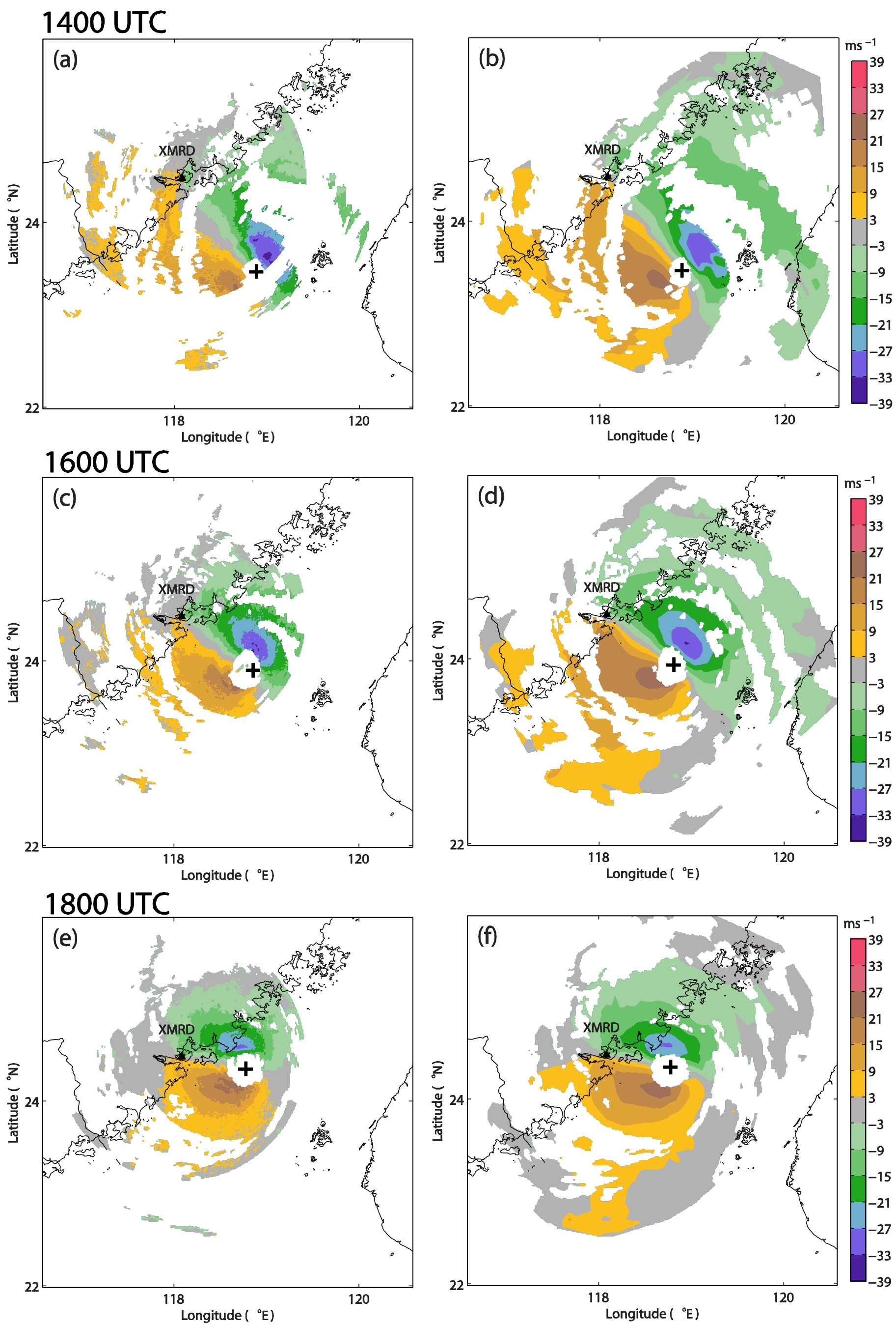

Fig. 13. (a, c, e) Observed radial velocity and (b, d, f) the radial velocity calculated from T-TREC winds at 3 km height at 1400 UTC (1st row), 1600 UTC (2nd row) and 1800 UTC (3rd row), 9 September 2010. '+' denotes the center of vortex.

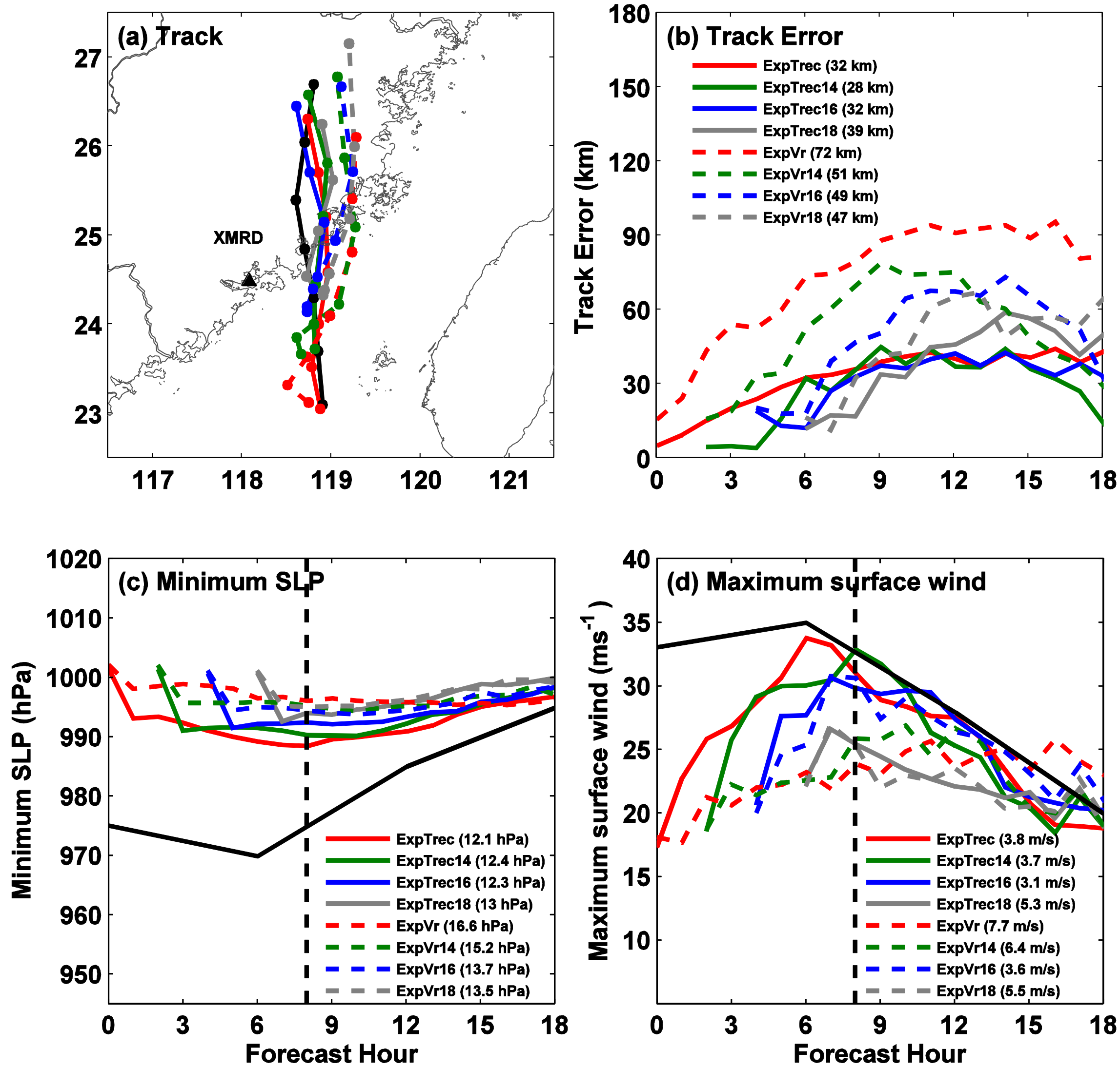

Fig. 14. The predicted (a) tracks, (b) track errors, (c) MSLP (hPa), and (d) MSW (m s^{-1}), for experiments ExpVr, ExpVr14, ExpVr16, ExpVr18, ExpTrec, ExpTrec14, ExpTrec16 and ExpTrec18. The numbers in (b), (c) and (d) represent the mean track errors, mean MSLP errors and mean MSW errors, respectively. The vertical dashed line in (c) and (d) represent the landfalling time for typhoon Meranti (2010).

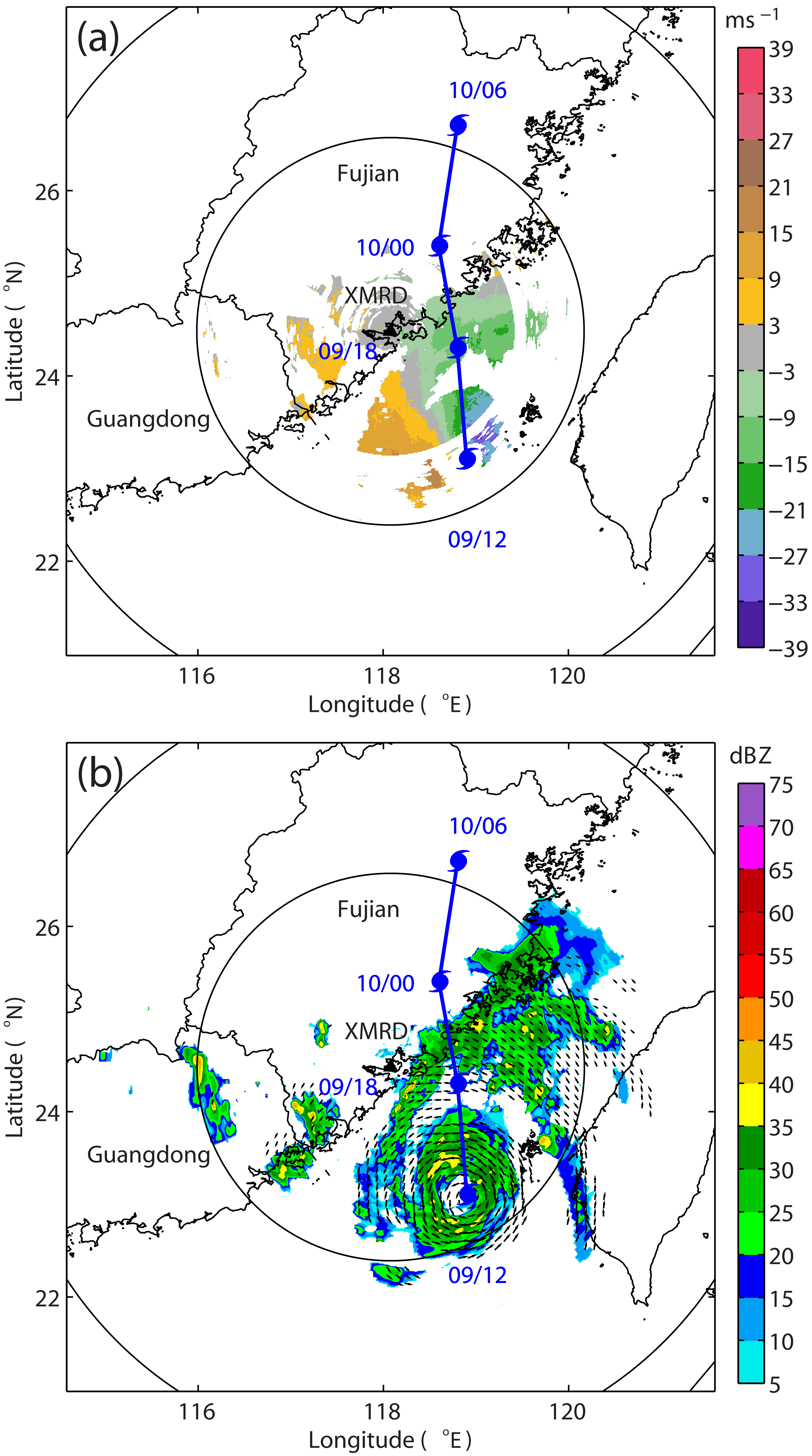

(a)
ms −1
39
33
27
21
15
9
3
−3
−9
−15
−21
−27
−33
−39
10/06
Fujian
10/00
XMRD
09/18
Guangdong
09/12
26
24
22
Latitude (°N)
116
118
120
Longitude (°E)
(b)
dBZ
75
70
65
60
55
50
45
40
35
30
25
20
15
10
5
10/06
Fujian
10/00
XMRD
09/18
Guangdong
09/12
26
24
22
Latitude (°N)
116
118
120
Longitude (°E)

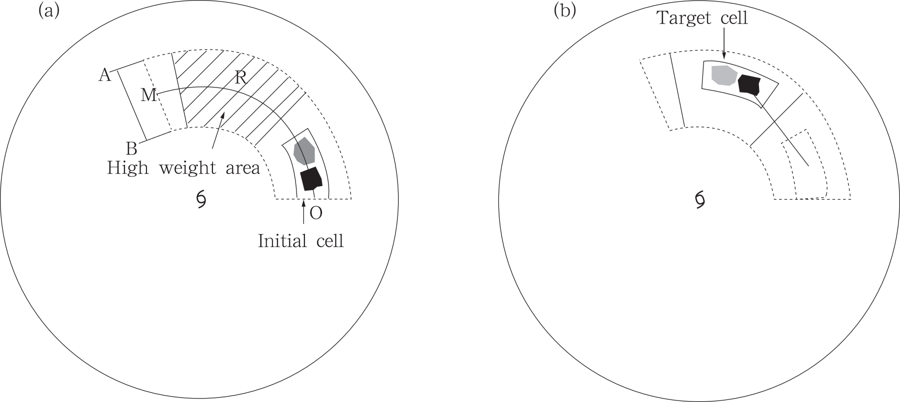

(a)
A
M
R
B
High weight area
O
Initial cell
(b)
Target cell

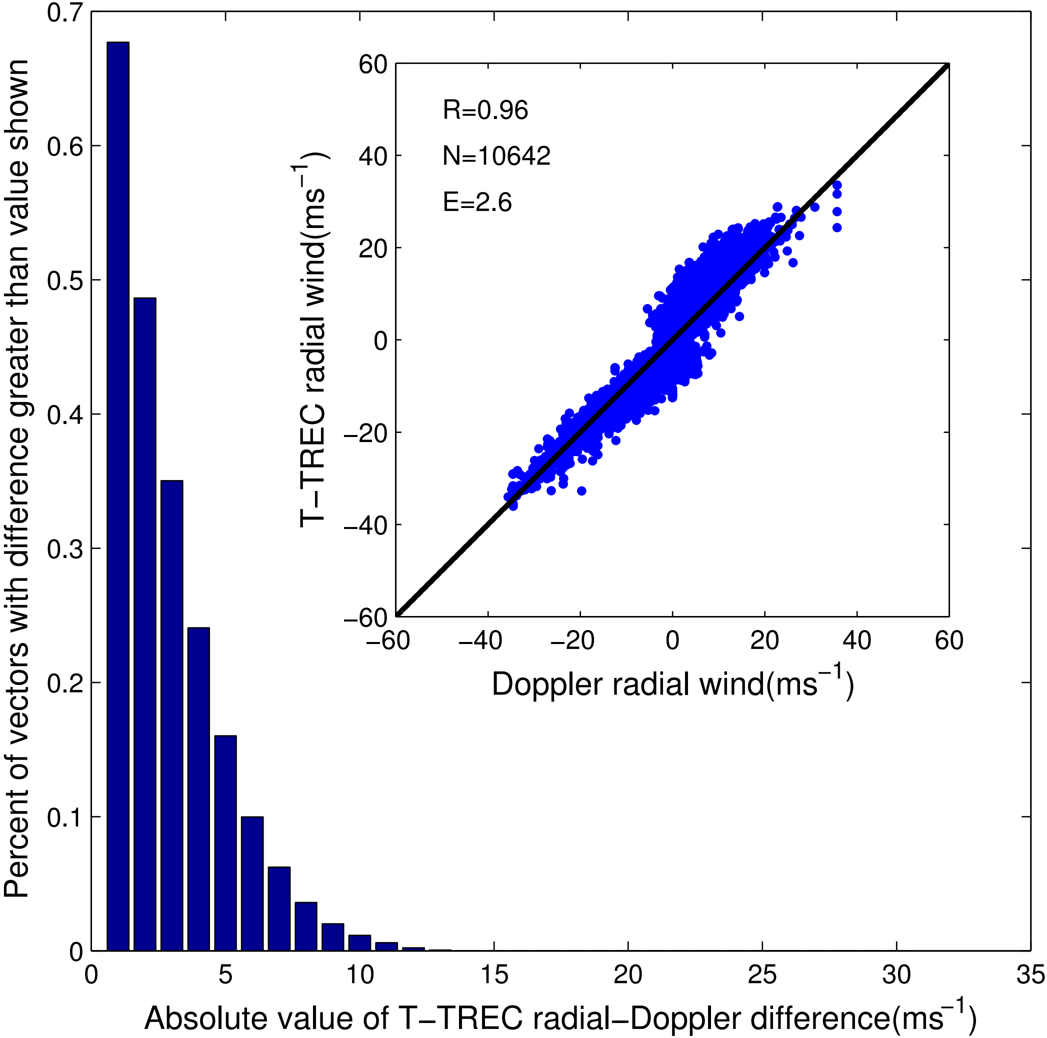

R=0.96
N=10642
E=2.6
T−TREC radial wind(ms^{-1})
Doppler radial wind(ms^{-1})
Percent of vectors with difference greater than value shown
Absolute value of T−TREC radial−Doppler difference(ms^{-1})

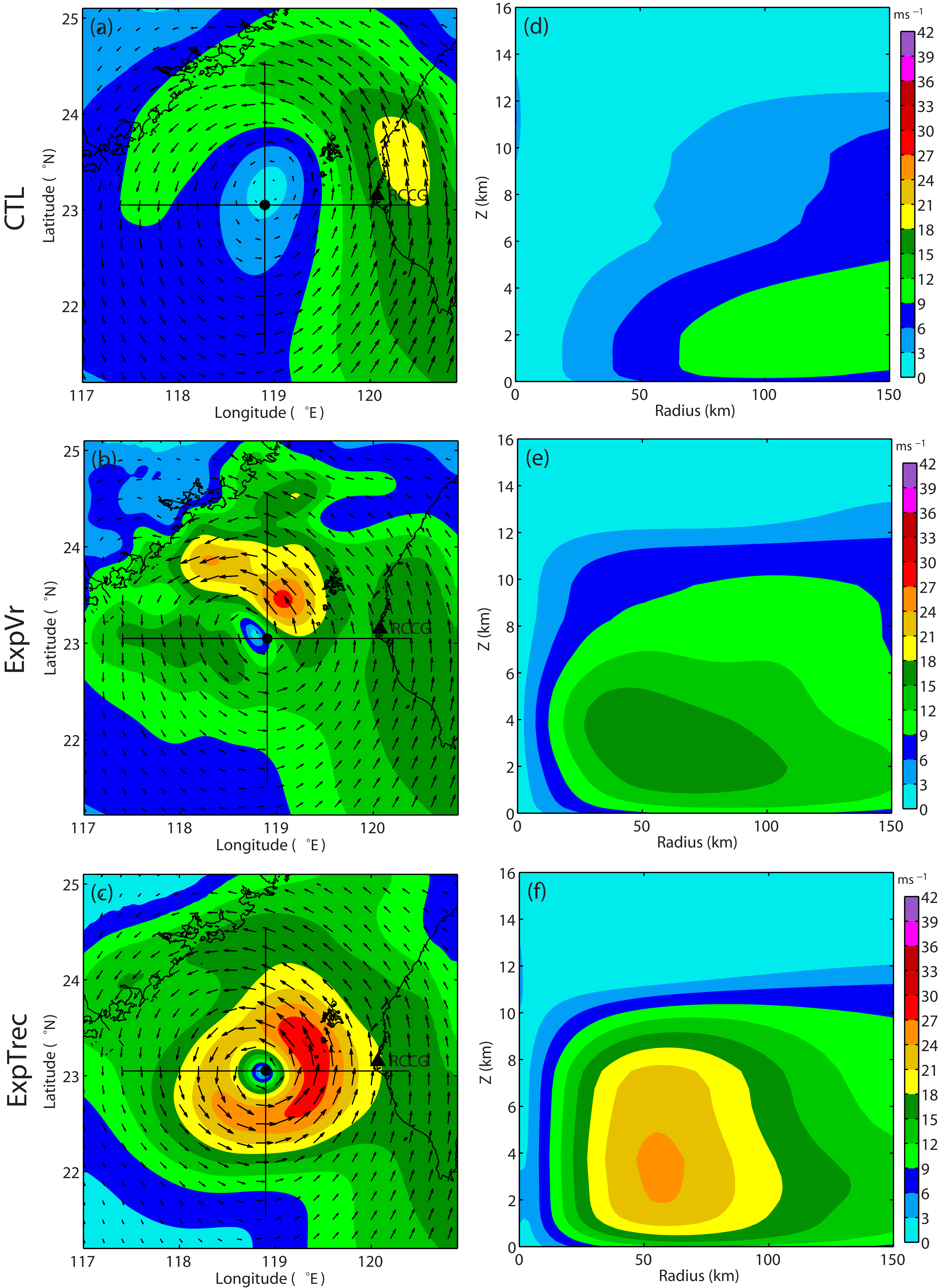

CTL
ExpVr
ExpTrec
(a)
(b)
(c)
(d)
(e)
(f)
RCCG
Latitude (°N)
Longitude (°E)
Z (km)
Radius (km)
ms −1
117
118
119
120
22
23
24
25
0
50
100
150
0
2
4
6
8
10
12
14
16
0
3
6
9
12
15
18
21
24
27
30
33
36
39
42

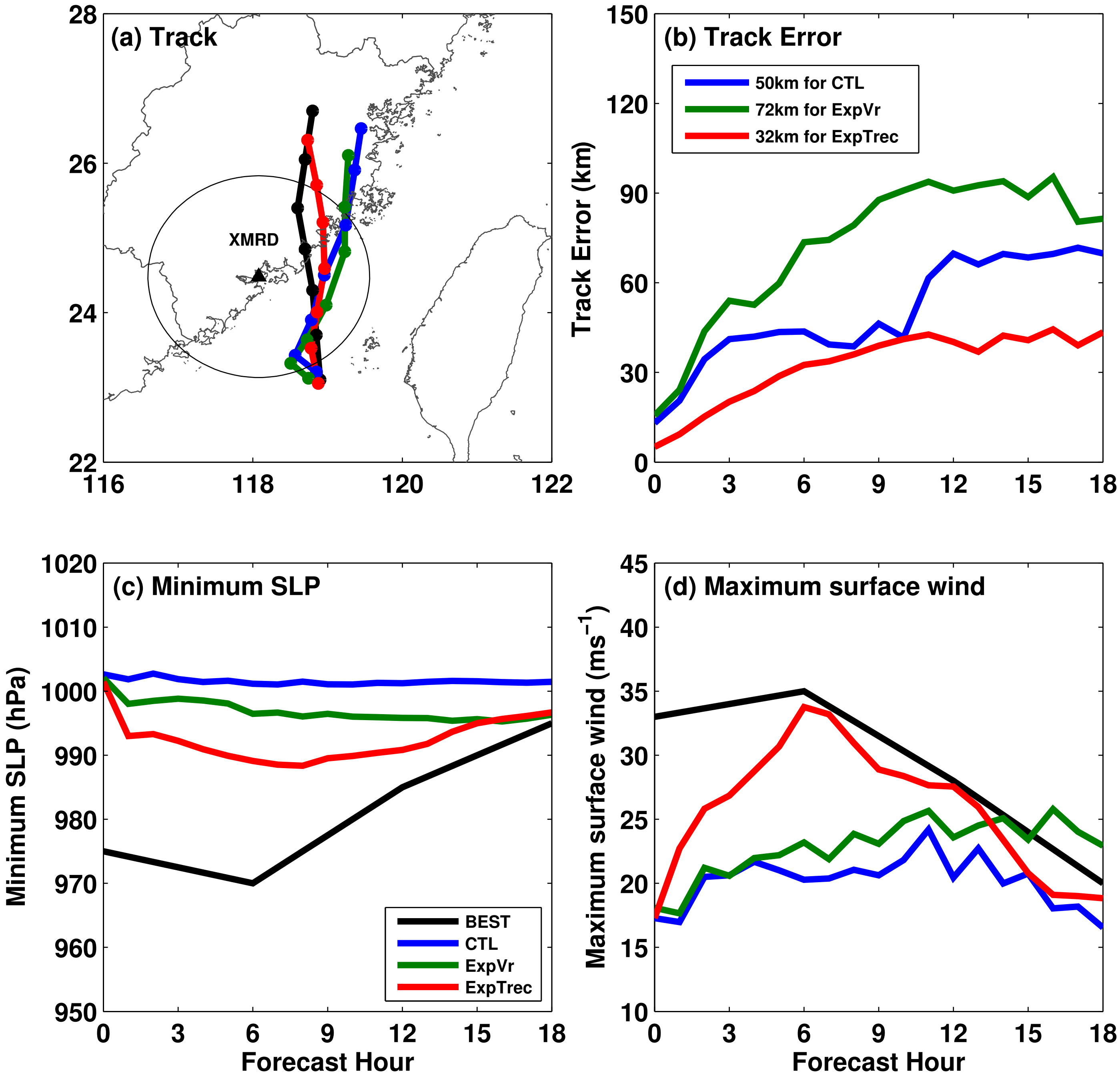

(a) Track
XMRD
28
26
24
22
116
118
120
122
(b) Track Error
50km for CTL
72km for ExpVr
32km for ExpTrec
Track Error (km)
0
30
60
90
120
150
0
3
6
9
12
15
18
(c) Minimum SLP
Minimum SLP (hPa)
950
960
970
980
990
1000
1010
1020
BEST
CTL
ExpVr
ExpTrec
Forecast Hour
(d) Maximum surface wind
Maximum surface wind (ms^{-1})
10
15
20
25
30
35
40
45
Forecast Hour

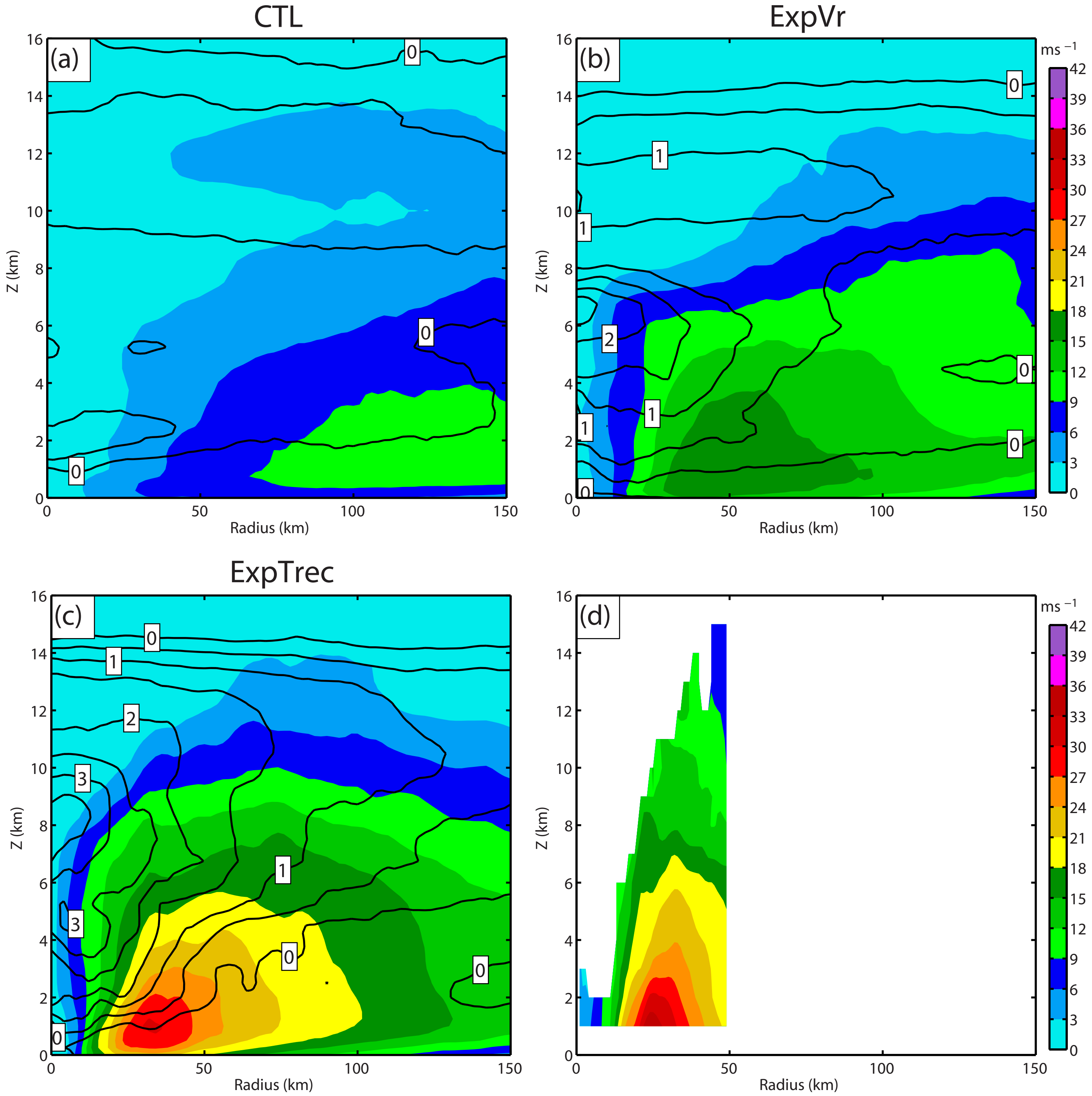
CTL
ExpVr
ExpTrec
(a)
(b)
(c)
(d)
Z (km)
Radius (km)
ms −1

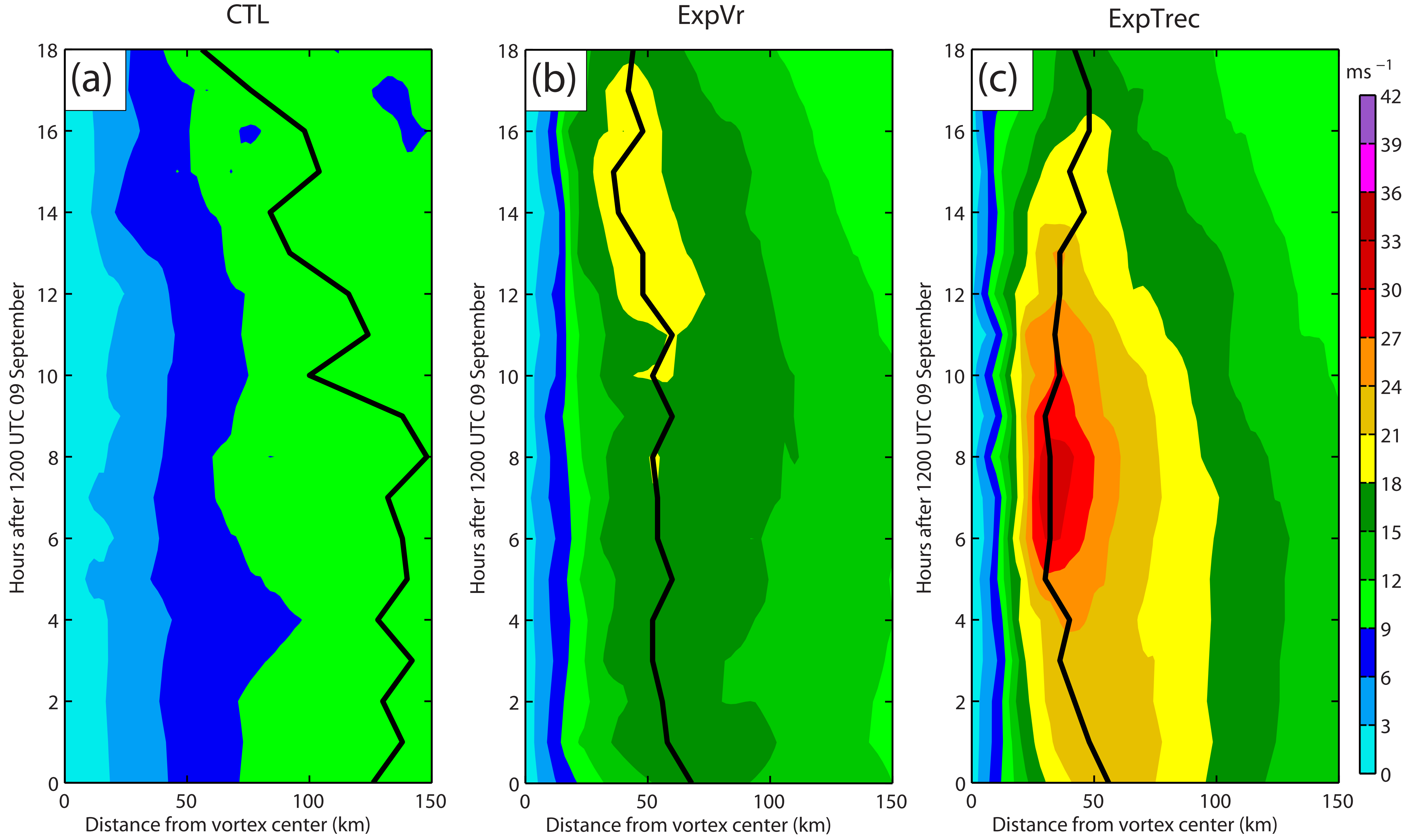

CTL
ExpVr
ExpTrec
(a)
(b)
(c)
Hours after 1200 UTC 09 September
Distance from vortex center (km)
0
50
100
150
0
2
4
6
8
10
12
14
16
18
ms −1
0
3
6
9
12
15
18
21
24
27
30
33
36
39
42

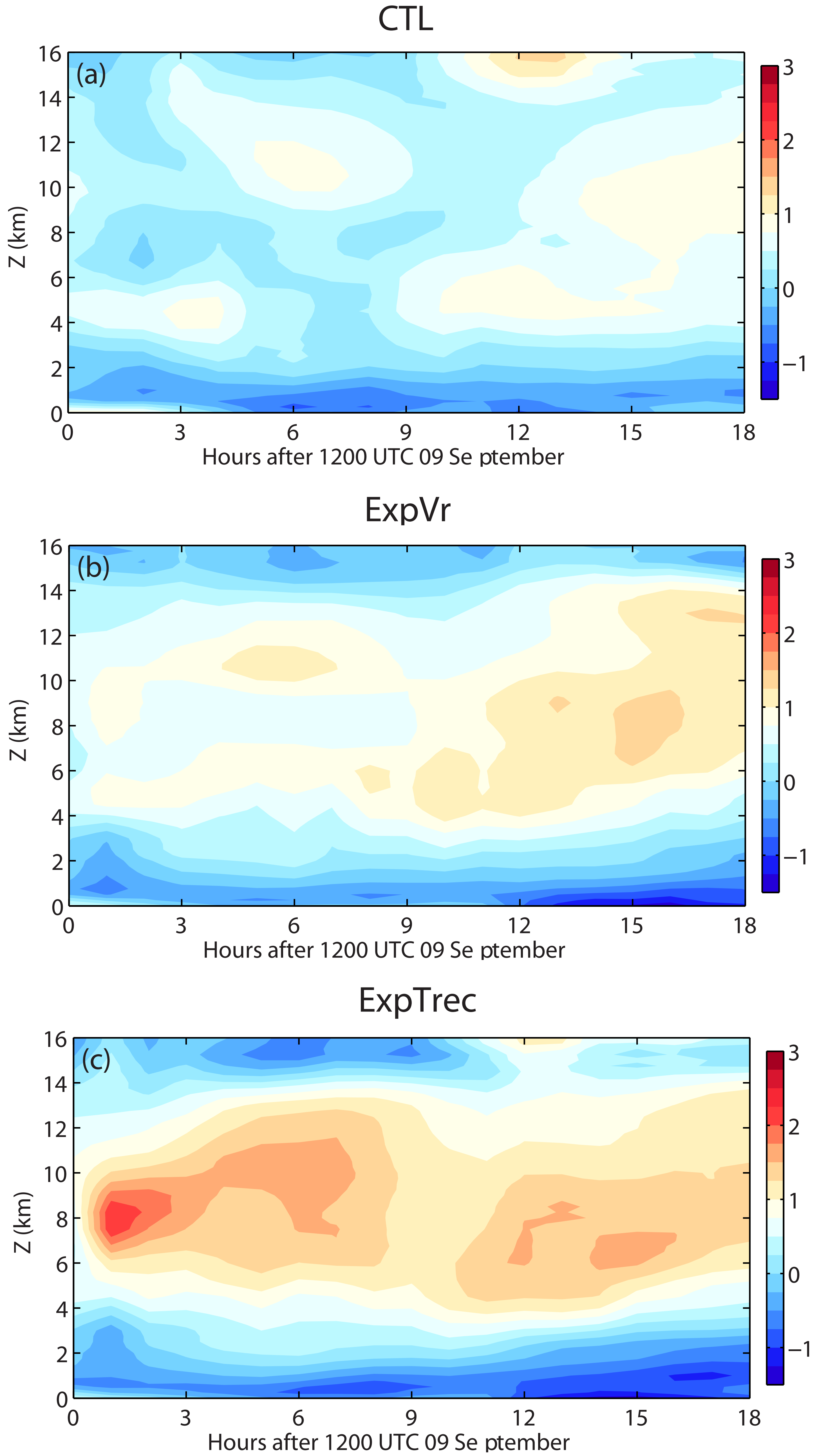
CTL
(a)
Z (km)
0
2
4
6
8
10
12
14
16
0
3
6
9
12
15
18
Hours after 1200 UTC 09 Se ptember
3
2
1
0
−1
ExpVr
(b)
Z (km)
Hours after 1200 UTC 09 Se ptember
ExpTrec
(c)
Z (km)
Hours after 1200 UTC 09 Se ptember

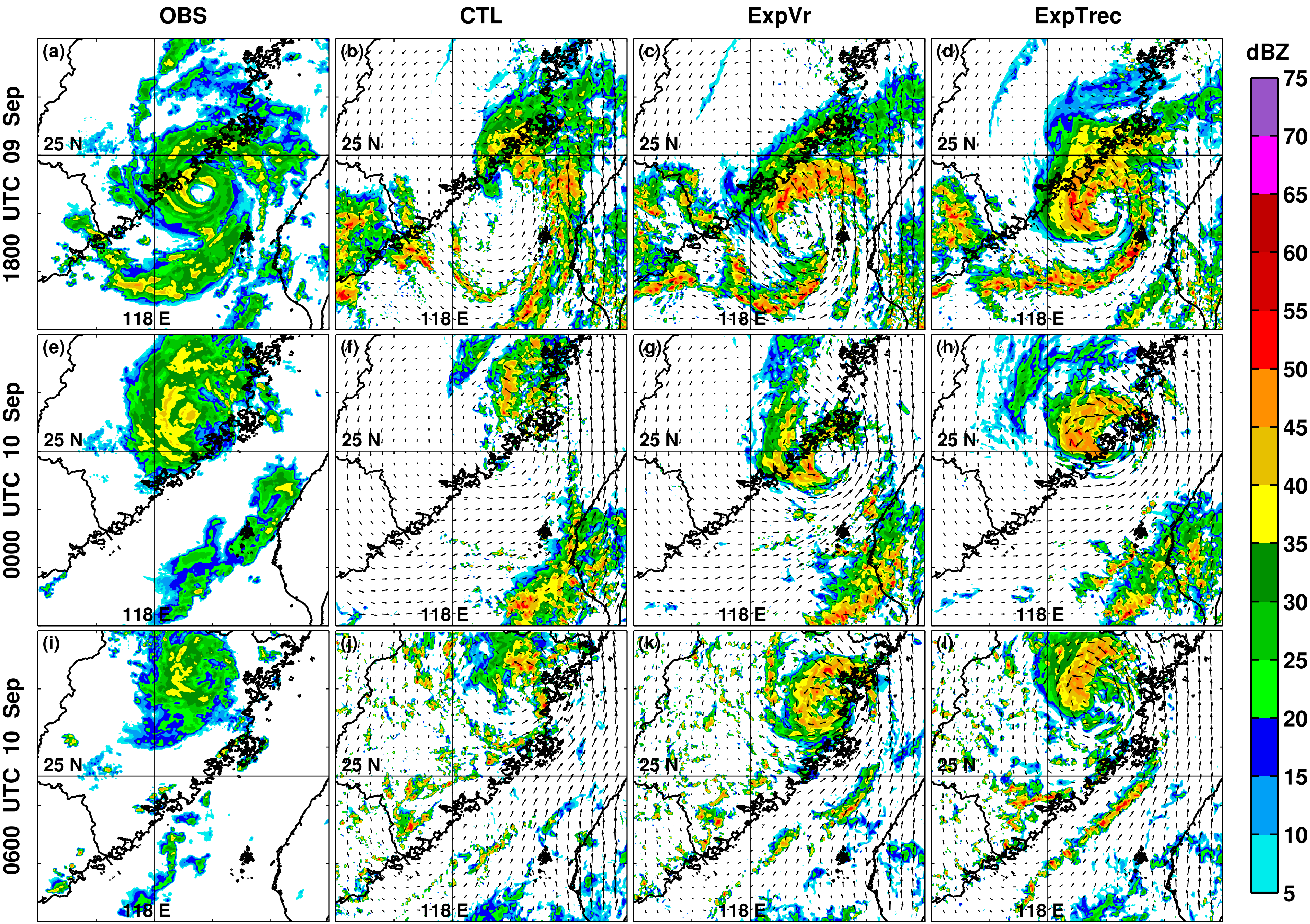

OBS
CTL
ExpVr
ExpTrec
dBZ
75
70
65
60
55
50
45
40
35
30
25
20
15
10
5
1800 UTC 09 Sep
0000 UTC 10 Sep
0600 UTC 10 Sep
(a)
(b)
(c)
(d)
(e)
(f)
(g)
(h)
(i)
(j)
(k)
(l)
25 N
118 E

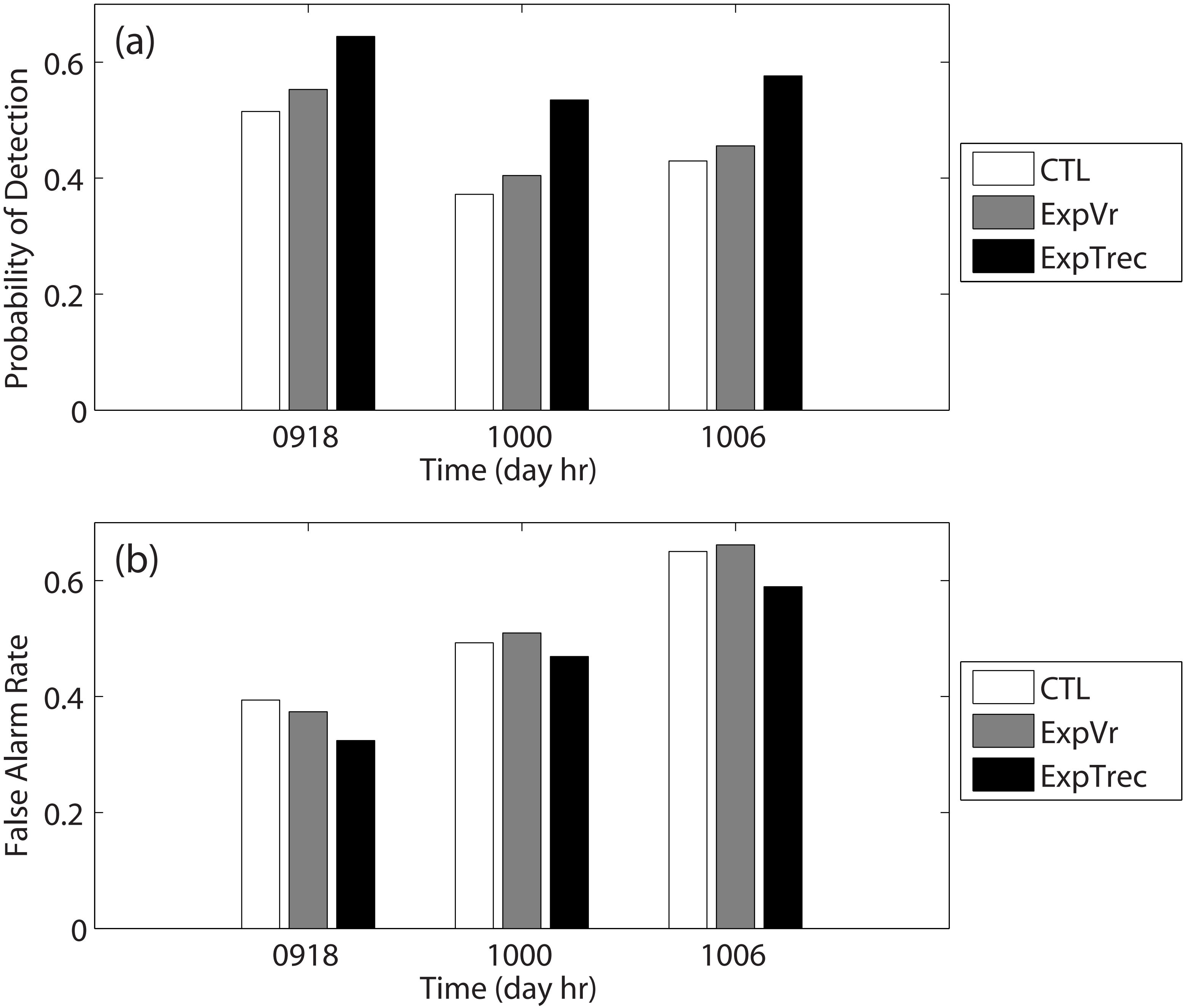
(a)
Probability of Detection
0
0.2
0.4
0.6
0918
1000
1006
Time (day hr)
CTL
ExpVr
ExpTrec
(b)
False Alarm Rate
0
0.2
0.4
0.6
0918
1000
1006
Time (day hr)
CTL
ExpVr
ExpTrec

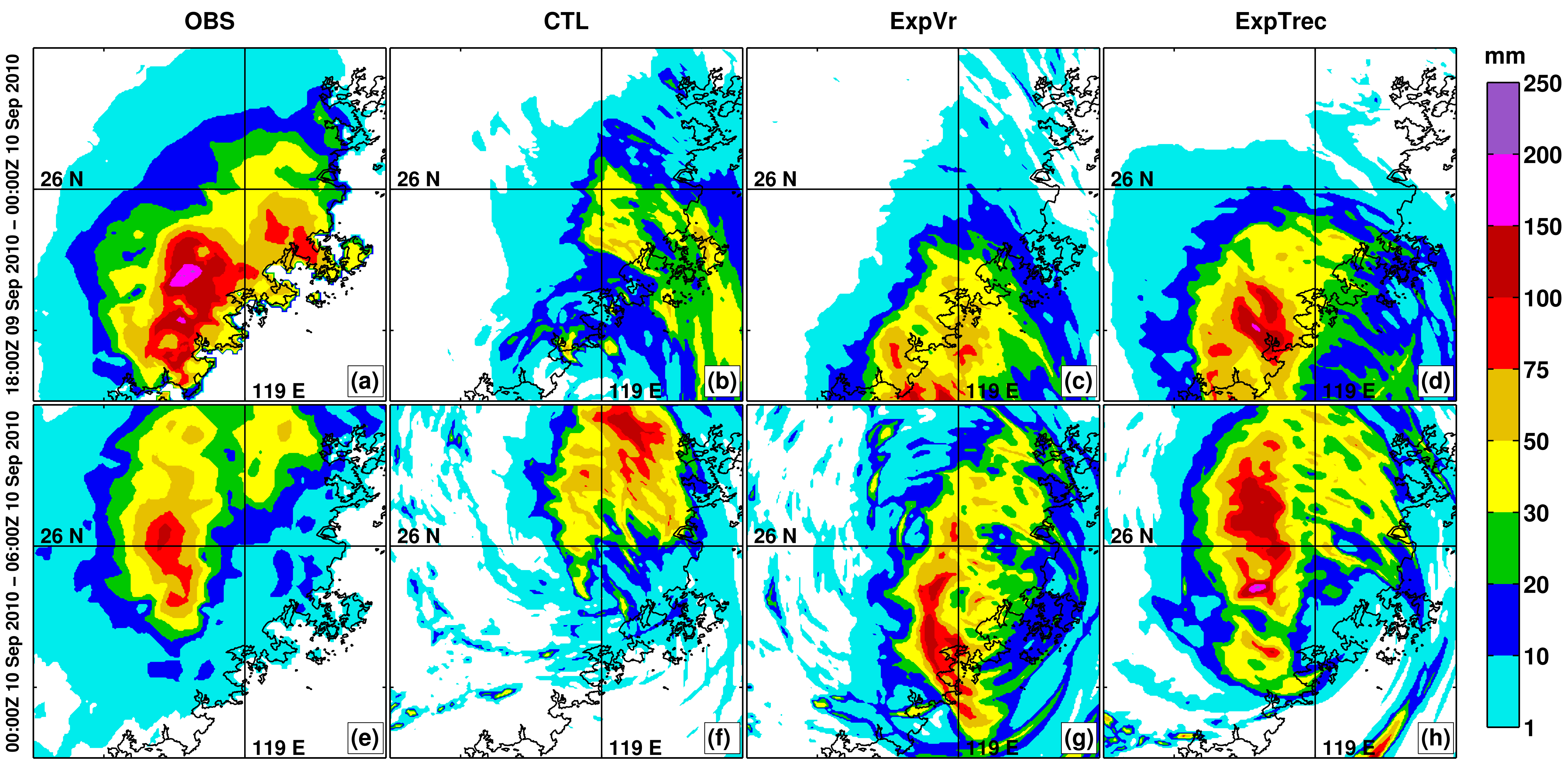

OBS
CTL
ExpVr
ExpTrec
18:00Z 09 Sep 2010 – 00:00Z 10 Sep 2010
00:00Z 10 Sep 2010 – 06:00Z 10 Sep 2010
26 N
119 E
(a)
(b)
(c)
(d)
(e)
(f)
(g)
(h)
mm
250
200
150
100
75
50
30
20
10
1

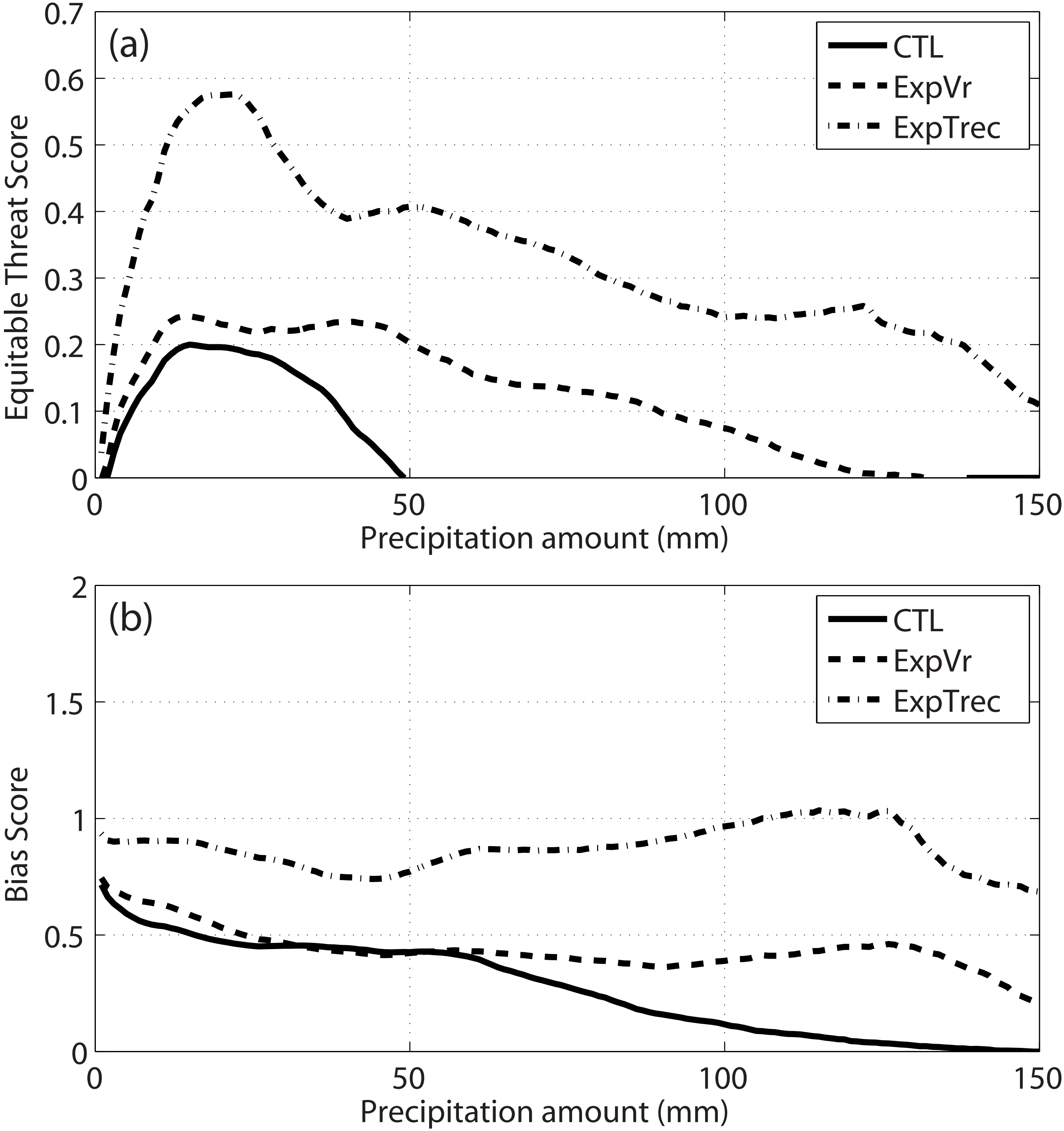

(a)
CTL
ExpVr
ExpTrec
Equitable Threat Score
Precipitation amount (mm)
0
0.1
0.2
0.3
0.4
0.5
0.6
0.7
50
100
150
(b)
CTL
ExpVr
ExpTrec
Bias Score
Precipitation amount (mm)
0
0.5
1
1.5
2
50
100
150

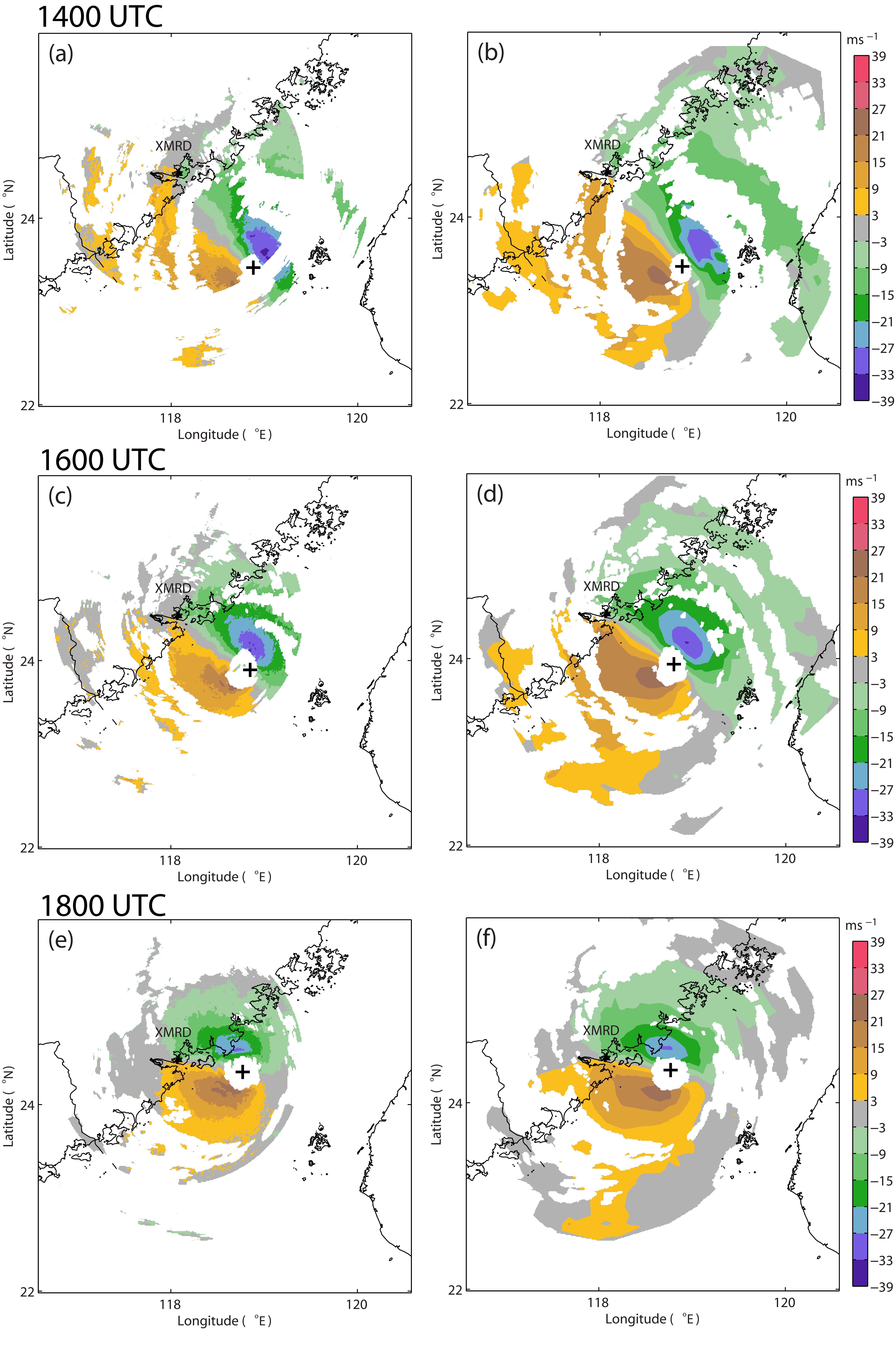
1400 UTC
(a)
(b)
1600 UTC
(c)
(d)
1800 UTC
(e)
(f)
XMRD
Latitude (°N)
Longitude (°E)
22
24
118
120
ms −1
39
33
27
21
15
9
3
−3
−9
−15
−21
−27
−33
−39

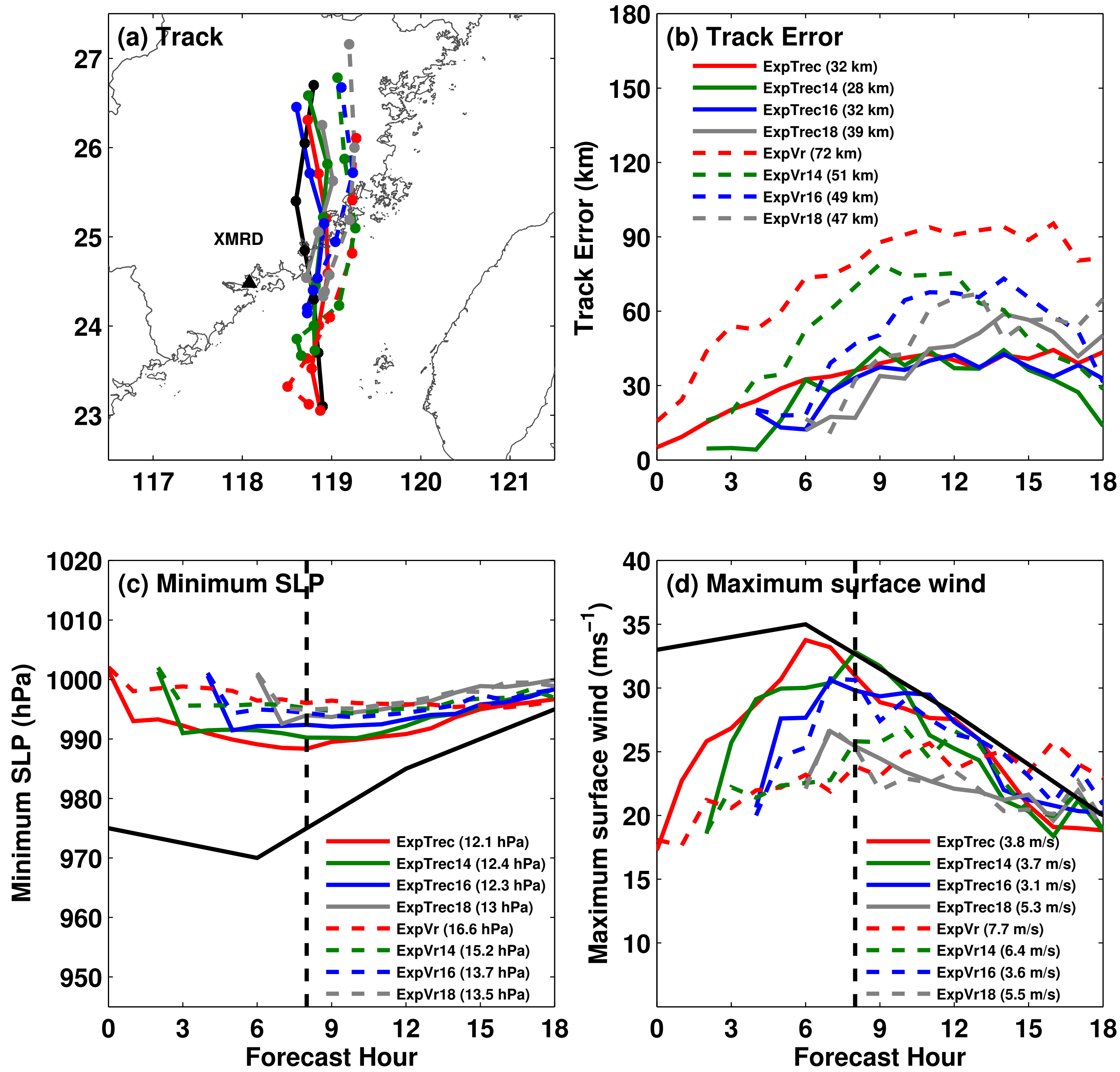
(a) Track
XMRD
117
118
119
120
121
23
24
25
26
27
(b) Track Error
ExpTrec (32 km)
ExpTrec14 (28 km)
ExpTrec16 (32 km)
ExpTrec18 (39 km)
ExpVr (72 km)
ExpVr14 (51 km)
ExpVr16 (49 km)
ExpVr18 (47 km)
Track Error (km)
(c) Minimum SLP
Minimum SLP (hPa)
ExpTrec (12.1 hPa)
ExpTrec14 (12.4 hPa)
ExpTrec16 (12.3 hPa)
ExpTrec18 (13 hPa)
ExpVr (16.6 hPa)
ExpVr14 (15.2 hPa)
ExpVr16 (13.7 hPa)
ExpVr18 (13.5 hPa)
Forecast Hour
(d) Maximum surface wind
Maximum surface wind (ms^{-1})
ExpTrec (3.8 m/s)
ExpTrec14 (3.7 m/s)
ExpTrec16 (3.1 m/s)
ExpTrec18 (5.3 m/s)
ExpVr (7.7 m/s)
ExpVr14 (6.4 m/s)
ExpVr16 (3.6 m/s)
ExpVr18 (5.5 m/s)
Forecast Hour